AJUR

American Journal of
Undergraduate Research

Volume 19 | Issue 1 | June 2022

www.ajuronline.org

Print Edition ISSN 1536-4585
Online Edition ISSN 2375-8732

AJUR
American Journal of
Undergraduate Research

Volume 19 | Issue 1 | June 2022

American Journal of Undergraduate Research (AJUR) *is a national, independent, peer-reviewed, open-source, quarterly, multidisciplinary student research journal. Each manuscript of AJUR receives a DOI number. AJUR is archived by the US Library of Congress. AJUR was established in 2002, incorporated as a cheritable not-for-profit organization in 2018. AJUR is indexed internationally by EBSCO and Crossref with ISSNs of 1536-4585 (print) and 2375-8732 (web).*

Myrica cerifera, a Medicinal Plant of the Lumbee Tribe, has Antibacterial and Nematicidal Properties

Ashley Edwards[*a], Kazhmiri Deberry[a], Hannah Mariani[a], Darian H. Taylor[b], Nicholas J. Cochran[b], Ana C. Barrios Sosa[b], Andrea Regan Scott[a], R. Thomas Williamson[b], Cornelia Tirla[c], Conner Sandefur[a], & Courtney Carroll Alexander[a]*

[a]Department of Biology, University of North Carolina at Pembroke, Pembroke, NC
[b]Department of Chemistry and Biochemistry, University of North Carolina Wilmington, Wilmington, NC
[c]Department of Chemistry, University of North Carolina at Pembroke, Pembroke, NC

https://doi.org/10.33697/ajur.2022.054

Students: ame029@bravemail.uncp.edu
Mentor: courtney.carroll@uncp.edu

ABSTRACT
Currently threatening the world of medicine is a growing number of antibiotic-resistant diseases. More specifically, bacteria and nematodes have gained resistance to many of the world's leading antibiotics and nematicides, respectively, making infections more difficult to treat. Subsequently, these parasitic organisms are able to continue damaging crops and other living organisms like humans without strong interference. To help people and the environment, the development of new and novel antibiotics is vital. Previous research suggests that phytochemicals are a potential solution that will not only help inhibit bacterial growth but also reduce nematode survival. We hypothesized that *Myrica cerifera*, a plant often used by the Lumbee tribe to treat illness, possesses antibacterial and nematicidal properties. To answer our hypothesis, we began by collecting plant specimens to extract material for biological assays and to subsequently isolate and elucidate the structures of active components. The extract was evaluated for antibacterial properties with an agar diffusion assay and then nematicidal properties using *Caenorhabditis elegans*. *M. cerifera* extract was added onto an agar lawn at various doses, and the nematodes' lifespans were scored. The findings of this study show that extracts of this plant, more commonly referred to as 'wax myrtle', do significantly decrease the lifespan of *C. elegans* and increase the zone of inhibition for *Staphylococcus epidermidis* and *Staphylococcus aureus*. In addition, two compounds were isolated and characterized through chemical extraction, chromatographic separation, and spectroscopic analysis. These compounds could potentially be used to treat bacterial and nematode infections.

KEYWORDS
Antibacterial; Antimicrobial; *Caenorhabditis elegans*; Plant extract; *Myrica cerifera*; Nematicidal; NMR; Phytochemical

INTRODUCTION

Bacteria are single-celled organisms found in every ecosystem on Earth. The human body itself is an ecosystem for bacteria. Remarkably, there are approximately thirty-nine trillion bacteria in the human body.[1] While many bacteria are non-pathogenic and even aid our digestive system in breaking down food, some are pathogenic. Pathogenic bacteria can cause crop damage, food spoilage, and a plethora of diseases.[2] In order to survive, however, bacteria have become resistant to extreme temperatures and UV radiation, which makes destroying them exceptionally challenging.[2]

Similarly, nematodes, also called roundworms, are mainly free-living organisms, but the few parasitic nematodes survive at the expense of the host.[3] Humans are hosts for approximately 300 species of parasitic worms.[4] According to the CDC, an upwards of 1.2 billion people are infected with *Ascaris* globally, which is only one genus of nematode.[5] While there are drugs to treat these infections, a lack of healthcare, sanitation, and growing resistance to the small number of drugs currently available, causes the proportion of the population infected to proliferate.[6] Relatedly, parasitic nematodes are also responsible for destroying crops, collectively costing approximately $80-$118 billion in crop damage.[7] The range of plants damaged by parasitic nematodes include, but are not limited to, agronomic and vegetable crops, foliage plants, and fruit and nut trees.[8] This damage is jointly caused by the 4100 species of nematodes that have been identified as plant parasites.[9] The main nematodes responsible for plant damage typically stem from order Tylenchida, and while *C. elegans* fall under order Rhabditida; both orders are classified as family

Rhabditidae.[7, 10] As such, chemicals that reduce *C. elegans* survival are likely to have similar effects on nematodes within that family, given that organisms within a family often share similar gene sequences and functional domains.

To protect our health and food crops, compounds that kill either bacteria or nematodes are invaluable. However, microbial resistance to classic antibiotics is an increasing dilemma. Resistance to antibiotics occurs as a result of natural selection, which is when bacteria with an adaptive mutation survive and continue to reproduce, whereas the bacteria without the adaptive mutation are selected against.[11] Many treatments for life-threatening illnesses and operations rely on antibiotics, such as cancer therapy and amputations.[12] According to a survey of oncologists in the United Kingdom, nearly 50% claim chemotherapy will soon be unviable due to antibiotic resistance.[13] For example, when the immune system is already compromised from chemotherapy, an antibiotic resistant disease like methicillin-resistant *Staphylococcus aureus* (MRSA) can be especially fatal.[14] An additional major cause of infection in the hospital is *Staphylococcus epidermidis*, with one study showing that 46% of hospital infectious samples tested positive for *S. epidermidis*.[15] Unlike MRSA, which has resistance against primarily methicillin, all *S. epidermidis* strains in the previously mentioned study were resistant to three or more different kinds of antibiotics.[15]

Promisingly, plants have a fantastic diversity of phytochemicals, many of which differ from those present in existing antibiotics. New chemicals may be helpful in creating revolutionary antibiotics that bacteria won't be resistant to.[16] Using the same chemicals to create antibiotics increases the odds that bacteria will be resistant to the medication. Phytochemicals are chemicals isolated from the plants they naturally originate in, and they perform in numerous ways to improve health.[17] A few plants that have these antibacterial properties include clove, roselle, rosemary, and thyme.[18] Their shared chemical classes include terpenes and flavonoids, which other investigators have shown have antimicrobial activity.[18,19] In this paper, we focus on *Myrica cerifera*, more commonly referred to as wax myrtle. Wax myrtle is an evergreen tree that some Native American tribes in North Carolina craft into teas to combat illness,[20,21] more specifically skin irritation and ailments of the digestive system.[22,23] It was hypothesized if wax myrtle was responsible for helping people recover, then compounds in the plant may possess antibacterial and nematocidal properties.

METHODS AND PROCEDURES

Plant harvesting and aqueous extraction

Myrica cerifera cuttings were collected in Spring 2019 in Fayetteville, NC. Leaves were removed from plants, dried, and stored at room temperature until use. To generate 20% aqueous extracts for biological assays, 1 g of ground leaves were combined with 5 mL ddH_2O, mixed by vortex, incubated for 20 minutes at 70ºC, and filter sterilized. The 20% solution was diluted with ddH_2O to generate less concentrated extracts.

Chemical extraction

For chemical extraction, the dried plant material was ground to a powder. The plant material was extracted with hot water, with 100 mg of plant material boiled in 500 mL of water for one hour, providing the aqueous extract. Volumes of 100 mL aqueous solutions were extracted with 3 x 20 mL of Chloroform ($CHCl_3$), then 3 x 20 mL of methylene chloride (CH_2Cl_2), and finally with 3 x 20 mL of ethyl acetate. The organic solvents were evaporated under a vacuum and analyzed by low-resolution NMR. This approach was not successful, and a different method was employed. The solid residue, recovered after filtration of the hot water solutions, was left to percolate overnight with 100 mL of $CHCl_3$ and filtered again. The $CHCl_3$ solution was evaporated under vacuum using a rotatory evaporator to generate a mixture that was purified by flash column chromatography on silica gel using a 5% gradient methylene chloride (CH_2Cl_2) in hexane as eluent.

NMR and LC-MC

All NMR data were recorded on a Bruker Avance 500 [500 MHz)] instrument equipped with a 1.7 mm TXI probe and using $CDCl_3$ as the solvent. Electrospray Ionization mass spectra (EIMS) (HRMS) data for accurate molecular weight and MS/MS fragmentation were measured using a Xevo G2-XS QTof spectrometer in positive ion resolution mode controlled by MassLynx v4.1 software (Waters Corporation). Key parameters were capillary voltage 2.5 kV, sampling cone 80 V, and source offset 80 V, source temperature 120, desolvation temperature 550, cone gas flow 100 L/hr, and desolvation gas flow 800 L/hr.

Agar diffusion assays

Glycerol stocks of *Micrococcus luteus, Bacillus subtilis, Corynebacterium xerosis, Proteus vulgaris, Neisseria sicca, Staphylococcus aureus, and Staphylococcus epidermidis* were streaked onto nutrient agar plates (Fisher Scientific, Pittsburg, PA, USA), grown overnight at 37 ºC and stored at 4 ºC until use. The day prior to agar diffusion assays,[23] 3 mL aliquots of nutrient broth (Fisher Scientific, Pittsburg, PA, USA) were inoculated from streak plates and grown overnight at 37 ºC. Overnight cultures were spread via a sterile L-spreader on Mueller-Hinton (MH) agar (Fisher Scientific, Pittsburgh, PA, USA) plates. Filter discs were soaked in 20% aqueous extract or ddH_20 (vehicle). The disc was shaken gently to remove excess extract and placed on MH agar plates. After overnight

incubation at 37 ºC, zones of inhibition (region of no growth around each filter disc) were measured by taking the diameter of each zone and normalized by subtracting the 6 mm disc size from each measured diameter. All agar diffusion assays were repeated three times.

C. elegans husbandry
Initial *C. elegans* stocks are ordered from the *Caenorhabditis* Genetics Center (CGC) at the University of Minnesota. Once acquired, the stocks were grown and maintained using general handling methods.[25] The nematodes (wild-type, N2) shipped from the CGC were backcrossed four times before any experiments.

Survival Assay

Plates were prepared with standard normal growth agar, and wax myrtle was added to some of the agar at varying doses (0.1 mg/mL, 0.01 mg/mL, or 0.001 mg/mL) following autoclave. We added OP50-1 to the plates and allowed them to dry before killing the bacteria with UV exposure. Worms were then age-synchronized by bleaching following standard protocols.[26]. Eggs were placed on the NGA plates +/- wax myrtle. Unhatched eggs were counted at 24 hours following bleaching. Once the nematodes reached L4 maturity, they were plated onto corresponding wax myrtle, and fluorodeoxyuridine (50 μM FUdR) treated NGM plates. Worms were housed at 20 ºC.

Scoring lifespan

If the platinum tip of a worm pick did not trigger a touch response in a *C. elegans*, then the worm was scored as dead and removed from the plate. Worms were transferred to plates with fresh *E. coli* when their food source started to run low or approximately three days after they were last moved. Any worms missing or damaged from crawling on the plastic side of the petri dish were not scored and marked as 'lost.' The damaged worms were then removed from the plate. All 'lost' worms were censored from data analysis to avoid confounding variables affecting the results.

Statistical analysis
Growth inhibition by aqueous extracts was compared to a negative control using Dunnet's multiple comparison test, and p-values below 0.05 were considered statistically significant. Calculations were performed using GraphPad Prism.
For the lifespan analysis, the data gathered was compiled on GraphPad Prism. Then, the Log-rank test was used to determine significance, comparing the extract versus vehicle treatment. A p-value below 0.05 was considered statistically significant.

RESULTS

Chemical extraction
Following a series of unsuccessful attempts to separate the components in the aqueous solution, promising results were acquired from the organic extracts obtained from the solid residue that was isolated by filtration of the mixtures resulting from the boiling of the plant material. Two extracts were isolated: one in $CHCl_3$ (4.67 g) and one in CH_2Cl_2 (3.58 g). These extracts were purified by flash column chromatography on silica gel using a 5% gradient methylene chloride (CH_2Cl_2) in hexane as eluent. At the end of both chromatography columns, two compounds were isolated, and the TLC and low-resolution NMR showed that two different compounds were present. Of the two compounds discovered, one was named tcpl1, a yellow solid, 1.03 g, and the second was named tcpl2, a green-brown solid, 0.464 g were isolated and further purified.

Isolation
The waxy material (sample TCPL1, 0.1952 g) was dissolved in 15% ethyl acetate/85% hexanes (400 μL). The mixture was sonicated for 5-10 minutes at room temperature until a homogenous solution was obtained. Approximately 50 μL of the solution was charged across a preparative thin-layer chromatography plate (EMD plates, Silica Gel 60 F254, size 10x20 cm, layer thickness 250 μm), and the mixture was eluted with 15% ethyl acetate/85% hexanes at room temperature. The component at $R_f = 0.33$, which eluted as a yellow band, was scraped off the plate, and the recovered light-yellow solid was treated with 5 mL of ethyl acetate in a 20 mL scintillation vial. The insoluble silica gel was allowed to settle, and the supernatant was separated and passed through a glass pipette packed with glass wool. The process was repeated three times, and the combined supernatants were concentrated at room temperature under nitrogen to provide a light-yellow residue which was eluted from a C_{18} solid-phase extraction cartridge with 80% MeOH in H_20 and evaporated to dryness under nitrogen.

NMR structure elucidation
The structures of the two components of the mixture, present in a 4:1 ratio of Compound 1 to Compound 2, were identified using 1D ^1H, 1H-^1H COSY, ^1H-^{13}C HSQC, and ^1H-^{13}C HMBC experiments (**Figure 1**).

Compound 1. 2',4'-dihydroxy-3'-methyl-6'-methoxychalcone - ^{1}H NMR (500 MHz, $CDCl_3$) δ 13.61 (s, 1H), 7.99 (d, J = 15.7 Hz, 1H), 7.84 (d, J = 15.7 Hz, 1H), 7.68 – 7.62 (m, 1H), 7.50 – 7.35 (m, 4H), 3.66 (s, 3H), 2.16 (s, 3H), 2.13 (s, 3H). HR-ESI-MS (calculated 299.1283, found 299.1288, 1.7 ppm). The spectral data matched that given in previous reports.[27–29]

Compound 2. 5,7-dihydroxy-6,8-dimethylflavanone (demethoxymatteucinol) ^{1}H NMR (500 MHz, $CDCl_3$) δ 12.27 (s, 1H), 7.70 – 7.61 (m, 1H), 7.50 – 7.35 (m, 5H), 5.41 (dd, J = 12.8, 3.2 Hz, 1H), 3.04 (dd, J = 17.1, 12.9 Hz, 1H), 2.85 (dd, J = 17.1, 3.1 Hz, 1H), 2.08 (s, 3H), 2.08 (s, 3H). HR-ESI-MS (calculated 285.1127, found 285.1127, 0.0 ppm) The spectral data matched that given in previous reports.[28-31]

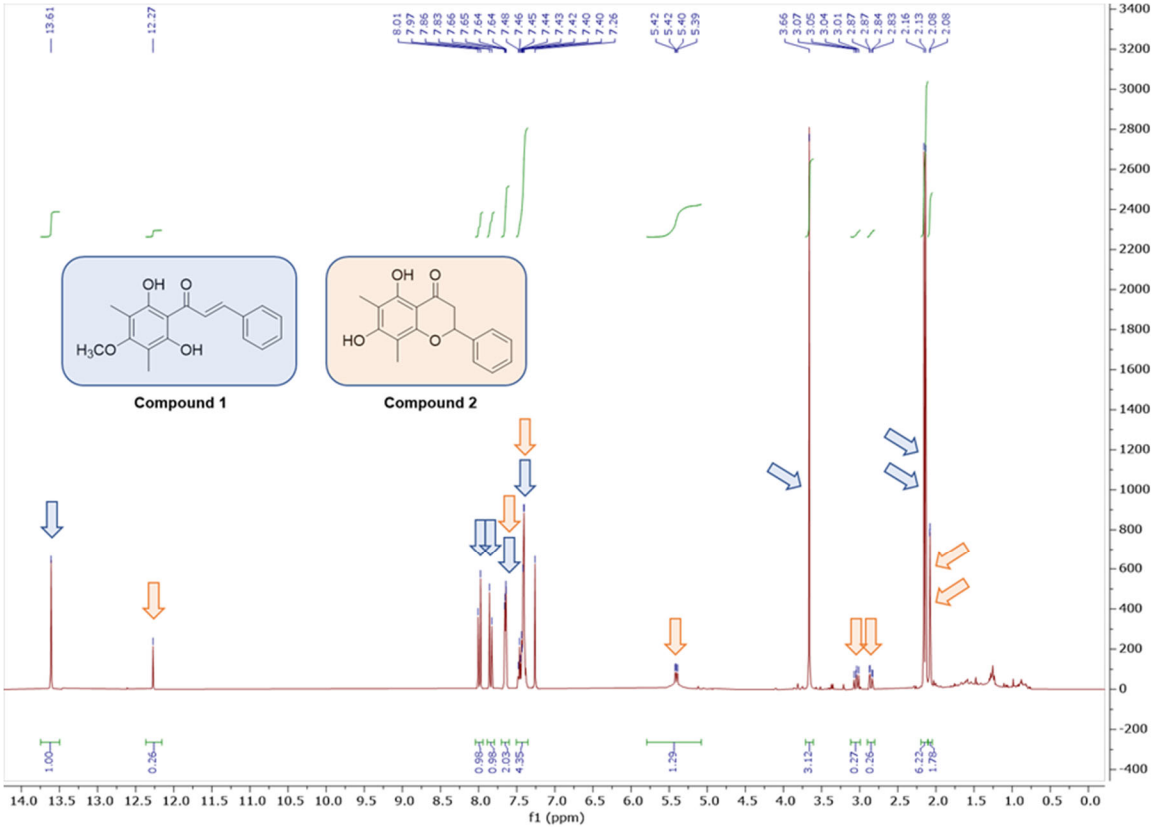

Figure 1. ^{1}H NMR of compounds 1 (blue) and 2 (orange).

Agar diffusion assay

To assess wax myrtle for antibacterial activity, we performed agar diffusion assays using extract against 13 common laboratory strains. Measured zones of inhibition were tested for statistical significance using GraphPad Prism. Aqueous-derived extract from wax myrtle significantly inhibited the growth of two of the 13 strains: *S. aureus* and *S. epidermidis* (**Figure 2**).

Nematicidal activity

To determine how wax myrtle affects *C. elegans* survival, we monitored plates of synchronous worms that were exposed to varying doses of wax myrtle extract and then compared them to vehicle-treated animals. The data gathered was compiled on GraphPad Prism. Then, a p-value of 0.006 was obtained from a Log-rank test. These results (**Figure 3**) reveal wax myrtle extract significantly decreased the survival of *C. elegans*, which was a trend observed in all three biological replicates. We also noted the percent of eggs unhatched compared to hatched nematodes on day one following treatment with wax myrtle. The results were compiled on GraphPad Prism, and a p-value of 0.0105 was obtained from a one-way repeated measures ANOVA test with Geisser-Greenhouse correction. The results (**Figure 4**) reveal wax myrtle significantly reduces the number of eggs that hatch at higher doses.

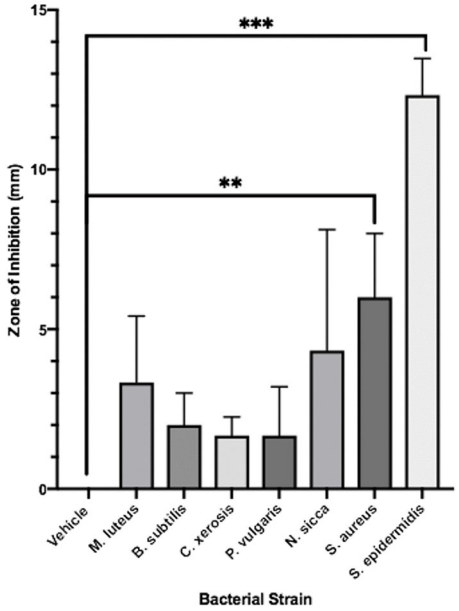

Figure 2. Agar diffusion assay showing bacterial inhibition by wax myrtle. Zone of inhibition (mm) of various bacterial strains by wax myrtle aqueous extract. The bacteria used in this assay include *Micrococcus luteus, Bacillus subtilis, Corynebacterium xerosis, Proteus vulgaris, Neisseria sicca, Staphylococcus aureus, and Staphylococcus epidermidis*. Bars represent the mean of three trials +/- SD. Statistical significance was calculated using a Dunnett's multiple comparison test against the vehicle treatment on Graph Pad Prism 8.0. ** p<0.01, *** p< 0.001, observations (n= 3).

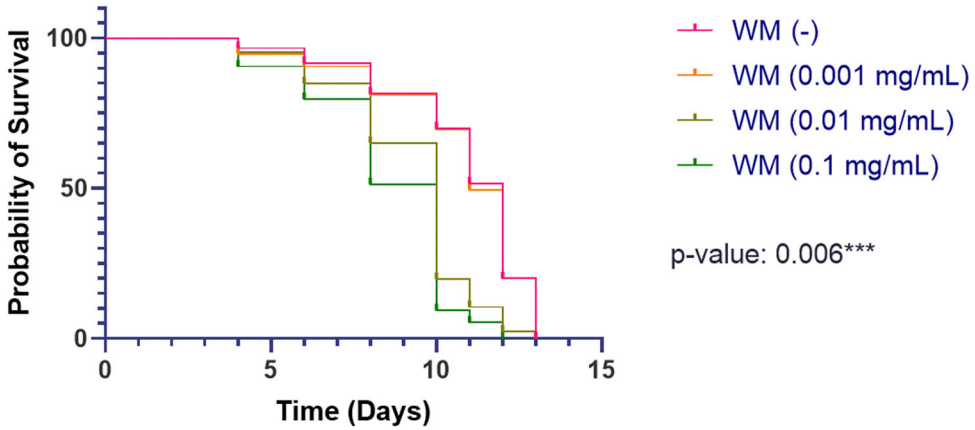

Figure 3. The effects of wax myrtle on *C. elegans* survival. The lifespan of *C. elegans* relative to time (days) in L4's maintained at 20 ºC. Values plotted are the number of dead worms per day after the initial treatment. Statistical significance was calculated with a Log-rank test on GraphPad Prism 8.0.0. *p=0.006, observations (n = at least 50 nematodes). The lifespan analysis was repeated two additional times for a total of 3 experimental replicates. The same trend was observed (see also Figures S1 and S2).

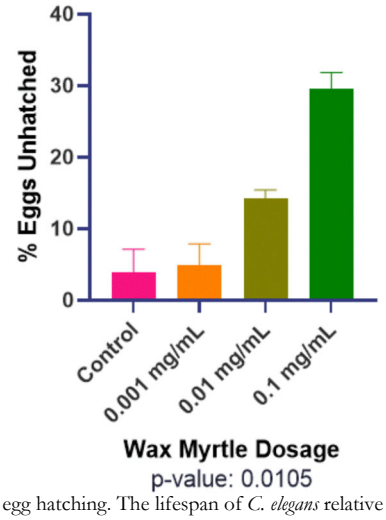

Figure 4. The effect of wax myrtle dosage on *C. elegans* egg hatching. The lifespan of *C. elegans* relative to time (days) in L4's maintained at 20 ºC. Values plotted are the number of eggs unhatched on day one following treatment. Statistical significance was calculated with a one-way repeated measure ANOVA test, with Giessen-Greenhouse correction on GraphPad Prism 8.0.0. *p=0.0105, observations (n = at least 50 nematodes). The bar graph is compiled from data gathered from three biological replicates.

DISCUSSION

This study began by examining the chemical properties of an herbal plant native to North Carolina, *Myrica cerifera.* Lumbee Indians, a Native American nation with homelands in southeast North Carolina, historically used and continue to use *M. cerifera*, also known as wax myrtle, as a medicinal plant to address digestive problems and skin irritation.[23] Several digestive issues (*e.g.,* inflammatory bowel disease, gastroesophageal reflux disease, and intestinal worms) are associated with microbial imbalance.[32,33] Additionally, bacteria, particularly *S. aureus,* underlie the majority of skin infections.[34] Therefore, we hypothesized that a plant used for generations to treat these types of digestive issues might possess antimicrobial properties.

Initially, we predicted there would be traces of terpenes and flavonoids in the chemical extraction, and the compounds we isolated confirmed our theory. The second compound was indeed a flavonoid. What we did not anticipate finding was a chalcone in the first compound, but chalcones are known to have antimicrobial activity as well as other beneficial biological activities.[35]

Our results confirm that the phytochemicals present in wax myrtle offer new antibacterial alternatives. In this experiment, we discovered wax myrtle extract significantly decreases the zone of inhibition for *S. epidermidis* and *S. aureus*. *S. epidermidis* is known for creating biofilms on catheters, and surgical implants,[36] whereas *S. aureus* is a common cause of skin and respiratory infections.[37] Furthermore, the emergence of methicillin-resistant *S. aureus* (MRSA) is an ongoing crisis in the medical community.[38] The development of new antibiotics is vital in decreasing the severity and number of cases for both species of staphylococcus bacteria.

Additionally, wax myrtle was found to contain compounds that reduce the lifespan of *C. elegans* as well as inhibit the growth of certain bacteria. More specifically, the plant extract significantly decreased longevity in wild-type (N2) *C. elegans*. Results shown in **Figure 3** have a p-value of 0.006%, denoting statistical significance. Wax myrtle's nematicidal properties are important because many current nematicides are toxic not only to nematodes but also to the plants and people they treat. A now banned nematicide called dibromochloropropane (DBCP) is hazardous to men because it's a testicular toxin. Another banned pesticide is aldicarb, which poisoned over 2,000 people in California in the early 1980s due to contamination.[39] More and more nematicides are getting banned due to unwanted toxicity at higher concentrations. Luckily, most phytochemicals are safer on the environment and humans than traditional chemical nematicides, so potential nematicides made from wax myrtle could provide a safer alternative for exterminating parasitic nematodes.[40] This can help cut down the billions of dollars wasted on crop damage and help combat the rising *Ascaris* infections. Our additional finding that wax myrtle significantly decreases fecundity, or the capability of *C. elegans* to produce offspring, further exemplifies why this evergreen shrub has potential as a nematicide. This capability to decrease fecundity is a trait shared by nematicide emamectin benzoate. Emamectin benzoate has been proven to be more effective than three other nematicides, which lack the ability to reduce the population by decreasing fecundity.[41]

In the future, we would want to determine what target(s) wax myrtle extracts attack the bacteria. *S. epidermidis* and *S. aureus* are gram-positive cocci arranged in grape-like clusters. These bacteria belong to Phylum Bacillales, which are correlated to the effectiveness of wax myrtle. That said, there was one more bacterium included in this assay belonging to Phylum Bacillales that was not significantly inhibited, *B. subtilis*. However, a critical difference is the genus of each bacterium. The two significantly inhibited bacteria are classified as genus *Staphylococcus,* whereas the bacteria that was not significantly inhibited is classified as genus *Bacillus*. The underlying molecular mechanism will be investigated.

Not only would we look into what targets the plant extract has, but we can also test structurally similar compounds to the extract. Moreover, we would like to continue testing survival, and other plant extracts on our extra wild-type (N2) nematodes and on mutant strains, particularly GC565 and BS3164. Both strains induce tumor formation in the germline at 25 ºC, which will be useful in evaluating the anti-cancer activity of the chalcones identified in the wax myrtle extract.[42,43] This will potentially provide us with knowledge on how the plant extracts shorten the lifespan of nematodes and what pathways the extract uses. In conclusion, wax myrtle's antibacterial and nematicidal properties will help shape future investigations in revolutionizing antibiotics and nematicides.

CONCLUSION

This study addresses the antibacterial and nematicidal effects of *Myrica cerifera*, more commonly known as wax myrtle. Our results show wax myrtle significantly decreases *C. elegans* lifespan and fecundity as well as the growth of *S. epidermidis* and *S. aureus*, indicating wax myrtle can alter how we develop antibiotics and nematicides in the future.

ACKNOWLEDGEMENTS

The authors thank the Lumbee Nation for sharing their traditional indigenous knowledge of *M. cerifera* through discussion and the informative text, *Herbal Remedies of the Lumbee Indians*, by Arvis Locklear Boughman and Loretta O. Oxendine.[23] We thank the NIGMS (National Institute of General Medical Sciences) for supporting the UNCP RISE Program by grant 5 R25 GM 77634-13, which subsequently funded this project. We also acknowledge and thank Dontae Moseley for helping start the *C. elegans* lab at UNCP and optimizing the related procedures.

REFERENCES

1. Sender, R., Fuchs, S., and Milo, R. (2016) Revised Estimates for the Number of Human and Bacteria Cells in the Body, *PLoS Biology. https://doi.org/10.1101/036103*

2. Killing Bacteria, Perdana University, *www.perdanauniversity.edu.my/killingbacteria/* (accessed Jan 2021)

3. About Parasites, Centers for Disease Control and Prevention, *www.cdc.gov/parasites/about.html#:~:text=A parasite is an organism,Protozoa* (accessed Jan 2021)

4. Cox, F. E. G. (2002) History of Human Parasitology, *Clinical Microbial Reviews* 15, 595–612. *https://doi.org/10.1128/CMR.15.4.595-612.202*

5. Parasites – Ascariasis, Centers for Disease Control and Prevention, *www.cdc.gov/parasites/ascariasis/index.html#:~:text=An estimated 807 million–1.2,-transmitted helminths (STH)* (accessed Feb 2021)

6. Stepek, G., Buttle, D. J., Duce, I. R., and Behnke, J. M. (2006) Human gastrointestinal nematode infections: are new control methods required?, *International journal of experimental pathology* 87, 325–341. *https://doi.org/10.1111/j.1365-2613.2006.00495.x*

7. Bernard, G. C., Egnin, M., and Bonsi, C. (2017) The Impact of Plant-Parasitic Nematodes on Agriculture and Methods of Control, *InTechOpen. https://doi.org/10.5772/intechopen.68958*

8. Nematode Diseases of Plants, Ohioline CFAES, *https://ohioline.osu.edu/factsheet/plpath-gen-8#:~:text=A%20number%20of%20genera%20and,%2C%20turfgrass%2C%20and%20forest%20trees* (accessed May 2021)

9. Decraemer, W., and Hunt, D. (2006) Structure and classification, in *Plant Nematology* (Perry, R., and Moens, M.) 3–32, CABI, Wallingford.

10. Smythe, A. B., Holovachov, O., and Kocot, K. M. (2019) Improved phylogenomic sampling of free-living nematodes enhances resolution of higher-level nematode phylogeny, *BMC Evolutionary Biology* 19. *https://doi.org/10.1186/s12862-019-1444-x*

11. About Antibiotic Resistance, Centers for Disease Control and Prevention, *www.cdc.gov/drugresistance/about.html* (accessed Feb 2021)

12. Oncologists Fear Rising Antibiotic Resistance Will Make Cancer Treatments Less Effective, The Pew Charitable Trusts, *www.pewtrusts.org/en/research-and-analysis/articles/2020/03/11/oncologists-fear-rising-antibiotic-resistance-will-make-cancer-treatments-less-effective* (accessed Feb 2021)

13. Effectiveness of Cancer Treatments Threatened by Rising Antibiotic Resistance, Longitude Prize, https://*longitudeprize.org/resources/effectiveness-cancer-treatments-threatened-rising-antibiotic-resistance* (accessed Feb 2021)
14. Managing and Treating Infections, American Cancer Society, *www.cancer.org/treatment/treatments-and-side-effects/physical-side-effects/low-blood-counts/infections/causes-germs-and-treatment-of-infections-in-people-with-cancer.html* (accessed Mar 2021)
15. Chabi, R., and Momtaz, H. (2019) Virulence factors and antibiotic resistance properties of the *Staphylococcus epidermidis* strains isolated from hospital infections in Ahvaz, Iran, *Tropical Medicine and Health* 47. *https://doi.org/10.1186/s41182-019-0180-7*
16. Borges, A., Abreu, A. C., Dias, C., Saavedra, M. J., Borges, F., and Simoes, M. (2016) New Perspectives on the Use of Phytochemicals as an Emergent Strategy to Control Bacterial Infections Including Biofilms, *Molecules* 21. *https://doi.org/10.3390/molecules21070877*
17. Difference Between Antioxidants and Phytochemicals?, American Institute for Cancer Research. *https://www.aicr.org/resources/blog/healthtalk-whats-the-difference-between-an-antioxidant-and-a-phytochemical/* (accessed May 2021)
18. Gonelimali, F. D., Lin, J., Miao, W., Xuan, J., Charles, F., Chen, M., and Hatab, S. R. (2018) Antimicrobial Properties and Mechanism of Action of Some Plant Extracts Against Food Pathogens and Spoilage Microorganisms, *Frontiers in Microbiology* 9, 1-7. *https://doi.org/10.3389/fmicb.2018.01639*
19. Myrica cerifera, Herbal Monograph, *http://www.ndhealthfacts.org/wiki/Myrica_cerifera* (accessed Mar 2021)
20. Myrica Cerifera, North Carolina Extension Gardener Plant Toolbox, *plants.ces.ncsu.edu/plants/myrica-cerifera/* (accessed Feb 2021)
21. Star, A. E., Mabry, T. J., and Smith, D. M. (1978) Triangularin, a new chalcone from *Pityrogramma triangularis*, *Phytochemistry* 17, 586–587. *https://doi.org/10.1016/S0031-9422(00)89386-3*
22. Croom, E. M., Jr. (1982) Plants and Their Uses, in *Medicinal Plants of the Lumbee Indians*, 30-160, ProQuest Dissertations & Theses Global, Michigan.
23. Boughman, A. L., and Oxendine, L. O. (2004) Herbs and Their Uses by the Lumbee, in *Herbal Remedies of the Lumbee Indians*, 11–102, McFarland, North Carolina.
24. Bauer, A. W., Kirby, W. M. M., Sherris, J. C., and Turck, M. (1966) Antibiotic Susceptibility Testing by a Standardized Single Disk Method, *AJCP* 45, 493-496. *https://doi.org/10.1093/ajcp/45.4_ts.493*
25. Brenner, S. (1974) The Genetics of *Caenorhabditis elegans, Genetics* 77, 71–94.
26. Maintenance of *C. elegans,* WormBook, *http://www.wormbook.org/chapters/www_strainmaintain/strainmaintain.html* (accessed Mar 2021)
27. Salem, M. M., and Werbovetz, K. A. (2005) Antiprotozoal compounds from *Psorothamnus polydenius*, *Journal of Natural Products* 68, 108–111. *https://doi.org/10.1021/np049682k*
28. Dao, T-T., Tung, B-T., Nguyen, P-H., Thuong, P-T., Yoo, S-S., Kim, E-H., Kim, S-K., and Oh, W-K. (2010) C-Methylated Flavonoids from *Cleistocalyx operculatus* and Their Inhibitory Effects on Novel Influenza A (H1N1) Neuraminidase, *Journal of Natural Products* 73, 1636–1642. *https://doi.org/10.1021/np1002753*
29. Mayer, R. (1990) Flavonoids from *Leptospermum scoparium*, *Phytochemistry* 29, 1340–1342. *http://doi.org/10.1016/0031-9422(90)85462-O*
30. Basnet, P., Kadota, S., Shimizu, M., Xu, H. X., and Namba, T. 2'-Hydroxymatteucinol, a New C-Methyl Flavanone Derivative from *Matteuccia orientalis*; Potent Hypoglycemic Activity in Streptozotocin (STZ)-Induced Diabetic Rat, *The Chemical and Pharmaceutical Bulletin* 41, 1790–1795. *https://doi.org/10.1248/cpb.41.1790*
31. Guarner, F., and Malagelada, J-R. (2003) Gut flora in health and disease, *Lancet* 361, 512–519. *https://doi.org/10.1016/S0140-6736(03)12489-0*
32. Corning, B., Copland, A. P., and Frye, J. W. (2018) The Esophageal Microbiome in Health and Disease, *Curr Gastroenterol Rep* 20. *https://doi.org/10.1007/s11894-018-0642-9*
33. Tong, S. Y. C., Davis, J. S., Eichenberger, E., Holland, T. L., and Fowler Jr., V. G. (2015) Staphylococcus aureus infections: epidemiology, pathophysiology, clinical manifestations, and management, *Clin Microbiol Rev. https://doi.org/10.1128/CMR.00134-14*
34. Mustafa, K., Perry, N. B., and Weavers, R. T. (2005) Lipophilic C-methylflavonoids with no B-ring oxygenation in *Metrosideros* species (Myrtaceae), *Biochemical Systematics and Ecology* 33, 1049–1059. *https://doi.org/10.1016/j.bse.2005.02.003*
35. Zhuang, C., Zhang, W., Sheng, C., Zhang, W., Xing, C., and Miao, Z. (2017) Chalcone: A Privileged Structure in Medicinal Chemistry, *Chemical Reviews* 117, 7762-7810. *https://doi.org/10.1021/acs.chemrev.7b00020*
36. Otto, M. (2009) *Staphylococcus epidermidis* – the "accidental" pathogen, *Nat Rev Microbiol* 7, 555-567. *https://doi.org/10.1038/nrmicro2182*
37. About *Staphylococcus aureus*, Minnesota Department of Health, *https://www.health.state.mn.us/diseases/staph/basics.html* (accessed May 2021)

38. Deadly Staph Infections Still Threaten the U.S., Centers for Disease Control and Prevention, *https://www.cdc.gov/media/releases/2019/p0305-deadly-staph-infections.html* (accessed May 2021)
39. Burns, A. R., Bagg, R., Yeo, M., Luciani, G. M., Schetzberg, M., Fraser, A. G., and Roy, P. J. (2017) The novel nematicide wact-86 interacts with aldicarb to kill nematodes, *PLoS Neglected Tropical Diseases. https://doi.org/10.1371/journal.pntd.0005502*
40. Chitwood, D. J. (2002) Phytochemical Based Strategies for Nematode Control, *Annual Review of Phytopathology* 40, 221–249. *https://doi.org/10.1146/annurev.phyto.40.032602.130045*
41. Bi, Z., Gong, Y., Huang, X., Yu, H., Bai, L., and Hu, J. (2015) Efficacy of Four Nematicides Against the Reproduction and Development of Pinewood Nematode, *Bursaphelenchus xylophilus*, *J Nematol.,* 47, 126-32. *https://www.ncbi.nlm.nih.gov/pubmed/26170474*
42. Strain Information, Caenorhabditis Genetics Center, *https://cgc.umn.edu/strain/BS3164* (accessed May 2021)
43. Strain Information, Caenorhabditis Genetics Center, *https://cgc.umn.edu/strain/GC565* (accessed May 2021)

ABOUT STUDENT AUTHORS

Ashley Edwards will graduate from the University of North Carolina at Pembroke in the Fall of 2022 with a BS in biology, a BS in chemistry, and a BA in music. She conducted this research to gain firsthand experience in a laboratory and learn about *C. elegans* husbandry. She feels this will better prepare her for a Ph.D. program following graduation. In addition to maintaining her passion for music, she hopes to work more with *C. elegans* in the future.

Kazhmiri Deberry will graduate from the University of North Carolina at Pembroke in the Spring of 2023 with an RN-BSN. She is enthusiastic about helping others and will use her science training in her future career.

Hannah Mariani graduated from the University of North Carolina at Pembroke in Fall 2020 with a BS in biology. She is currently applying to MPH programs and credits her work in the research lab with developing her scientific skills.

Darian Higgins is a senior at the University of North Carolina at Wilmington who is planning to graduate in May of 2021. Her major is Exercise Science, with a concentration in Allied Health. Darian is enthusiastic about becoming a pharmacist, and she is excited that the research work she completed through the collaboration with UNC Pembroke allowed her to integrate firsthand laboratory aspects of pharmaceutical science into her career path.

Nicholas Cochran will graduate from the University of Wilmington in the Summer of 2021 with a major in Biology and a minor in Chemistry. The work he completed through the collaboration with UNC Pembroke inspired him to continue doing research in Pharmaceutical Chemistry, and he now plans to pursue a career in this field.

PRESS SUMMARY

This study looks into the antibacterial and nematicidal effects of an evergreen tree, more specifically known as wax myrtle. Our results show wax myrtle significantly decreases lifespan in roundworms and the growth of certain bacteria. This suggests that wax myrtle can improve how scientists develop antibiotics and nematicides in the future.

State Adoption of Cryptocurrency: a Case Study Analysis of Iran, Russia, and Venezuela

*Rose Mahdavieh**

Department of Political Science, University of Central Florida, Orlando, FL

https://doi.org/10.33697/ajur.2022.055

Student: rosemahdavieh@knights.ucf.edu
Mentor: anca.turcu@ucf.edu

ABSTRACT
The emergence of digital currency is becoming prevalent in the age of globalization – specifically, cryptocurrencies, a subset of digital currency that encompass revolutionary technology. This study postulates that certain governments are more prone to adopting cryptocurrencies, especially those seeking to eschew international sanctions and protect corrupt practices. Three comparative case studies focus on countries (Iran, Russia, and Venezuela) that share attributes that result in adopting what has been called "native cryptocurrencies": corruption, GDP level, economic volatility, and Western sanctions.

KEYWORDS
Cryptocurrency; Blockchain; Political Science; Law; Foreign Sanctions; Government; Iran; Russia; Venezuela

INTRODUCTION

The adoption of cryptocurrencies can foster inclusiveness through increased transparency or manipulation to further corruption. What motivates certain countries to adopt native, government-backed cryptocurrencies? This study examines governments that have expressed an interest in cryptocurrencies, the first global decentralized currencies, through groundbreaking and revolutionary technology that facilitates non-traditional currency transactions at a rapid pace. The celerity and originality of these new currencies may make them quite attractive to governments like Iran, Venezuela, and Russia (studied here) that feel constrained or shortchanged by established, traditional currency markets and mechanisms.

This article seeks to assess if cryptocurrency adoption by national governments is most likely to occur in states run by kleptocratic regimes and experiencing well-established challenges to their currency systems, such as U.S. sanctions, economic volatility, and the weight of a "resource curse" (resource-rich countries). I use the terms 'kleptocrat' and 'kleptocratic' according to usages found in the academic literature:[1] rulers and regimes that thrive due to practices that dispossess citizens of pecuniary and other resources, such as land. According to the authors, this is a trait quite common in developing countries that otherwise rely on extractive economies: "Many developing countries have suffered under the personal rule of 'kleptocrats,' who implement highly inefficient economic policies, expropriate the wealth of their citizens, and use the proceeds for their glorification or consumption" (p. 162).

Cryptocurrencies are a subset of digital, decentralized currencies that revolutionize traditional fiat systems as no one entity can control or manipulate the market. The ownership of each transaction is approved cryptographically by other nodes in the network system, forming the Distributed Ledger Technology (DLT), known as the blockchain.[1] Public blockchain ensures the ability to trace the history and application, making it impossible to commit fraud, manipulation, and corruption; this may increase trust in the system. Due to the transparency and high efficiency of public blockchain, each transaction is recorded and validated by multiple stakeholders, limiting corruption and manipulation in nation-states.[1] Private blockchain is similar to public blockchain in the peer-to-peer transactions and a consensus chain of blocks. However, a major distinguishing factor is permission entrance.[1] Unlike a public blockchain that has public transparency and accessibility to the ledger, private blockchain requires permission for the distributed ledger to be visible to those invited. Therefore, transactions are censored and can only be visible to the group. Private blockchains have the authorization to monitor all transactions made by the public. This allocates power in the hands of those invited into the blockchain, allowing room for government control and corruption, and limiting transparency and accountability.[1] As opposed to global cryptocurrencies, native cryptocurrencies run on a private blockchain, which can foster kleptocracy and corruption as well as illicit conduct in efforts to strengthen the ruling elite resulting in expansion of powers and authoritarian politics.[2]

Native cryptocurrencies can push personal agendas of kleptocratic leaders through the private blockchain, only accessible to the issuing government (and invited authorities). This likely enhance corruption and allows kleptocratic behavior by certain states.[3]

The literature suggests that native cryptocurrencies tend to emerge in politically unstable countries that meet certain conditions: inflation, high economic volatility, and Western sanctions.[3] These conditions also seem to be prevalent in resource-rich countries with kleptocratic regimes in power. Kleptocracies have extractive economies, which are characterized as a small group of individuals controlling the domestic market in an effort to exploit the population.[4] They extract wealth from one subset of society to benefit another, restrain free market growth, limit public participation, and facilitate increased levels of corruption. Kleptocratic regimes with extractive economies abundant in resources are known as "resource cursed."

The resource curse theory holds that countries with a high abundance of natural resources have fewer opportunities for economic growth and democratic governance. In resource-rich countries, political instability occurs when such dysfunctional state policies are enforced, leading to mismanagement of resources and plummeting prices, therefore, hurting the economy.

Gabriel V. Rindborg[5] and Jules Hirschkorn et al.[6] both agree an important concept associated with resource-rich states is high economic volatility. In resource-rich countries with kleptocratic regimes, volatility creates instability attributable to high dependency on resources and the lack of economic diversification.

Another contributing factor that deters the economy is the mismanagement of resources, executed by the elites for corrupt intentions, which creates an inefficient economy.[7] Yadhollah Dadgar and Rouhollah Nazari[8] concluded most oil-producing countries are involved in economic corruption and described the foundations of economic corruption; the more transparent an economy is, the fewer opportunities for corruption.

Dadgar and Nazari[8] show that economic corruption can be combated through transparency and institutions that can function effectively. However, limiting economic corruption in kleptocracies is hard, especially if the kleptocratic authority has supremacy over all state resources, severely limiting the possibility of a transparent and inclusive economy.
According to Hirschkorn[6], cryptocurrencies offer a good chance of curing high economic volatility and enhancing nation-states' ability to break away from traditional systems without compromising security or legitimacy but rather increasing traceability and transparency. Robert Viglione[9] concludes cryptocurrencies allow greater economic freedom because of their decentralized nature and peer-to-peer transactions. He claims that citizens living under highly repressed economies that experience limited freedom, limited political participation, high trade barriers, and inflation tend to transmit funds into cryptocurrencies to maintain the current value of money. Governments fighting Western sanctions find cryptocurrencies appealing as they open more opportunities for economic trade globally. Viglione's statistics on Russia and Venezuela reveal both countries have relatively low economic investment and financial freedom.[9]

Inflation can prompt countries to issue government-backed cryptocurrencies in an effort to bolster the economy.[10] It is controlled by the central bank, which seeks to keep inflation rates within permissible boundaries so as not to harm the economy. There is a positive relationship between a government's budget deficit and inflation.[11]

Cryptocurrencies have become a viable solution that encompasses digital currency and cyber security capabilities while addressing inflation. Publicized cryptocurrencies are immune to hyperinflation, whereas native cryptocurrencies can be inflated in the hands of kleptocratic regimes that manipulate them for self-serving purposes.[1]

Western sanctions are another factor that can prompt the development of native cryptocurrencies. Considering some countries have an unstable economic system with inflation and devalued currency, sanctions intensify these symptoms, forcing governments to find alternative cures to alleviate the epidemic. Most sanctions imposed have the intention to put pressure on another nation to comply with Western ideology. In the long run, this policymaking and stigma of resorting to sanctions undermine the intended purpose of enforcing them in the first place. Kleptocratic regimes are coerced into finding an alternative, and cryptocurrencies emerge as such because they question the power of the dollar.[3]

Deane R. Konowicz[3] shows kleptocratic regimes are more likely to engage in digital currency theft due to their preexisting criminal enterprise behavior. He lists five cryptocurrency strategies that enable countries to circumvent U.S. sanctions; first, state-controlled cyber activities of stealing digital currencies are possible, especially in Russia, whose advanced cyber capabilities allow it to potentially access cryptocurrencies through cyber hacking.[2] Second, countries are experimenting with cryptocurrency mining, which is a process through which transactions are verified and added to the blockchain digital ledger. Governments can employ citizens to mine cryptocurrencies for them, free from reliance or interference from other countries. Third, a national cryptocurrency backed by resources is another solution that gives countries financial independence from U.S. sanctions. The

fourth strategy enables multiple states to form a common cryptocurrency, which will be revisited later in the paper in discussing BRICS. Finally, a state's population could resort to utilizing digital currencies freely because of the economic impact sanctions may create.[3] All these strategies are possible; however, the case-study countries are similar in their reliance on resources, which makes the third strategy most attractive. Thus, for the purposes of this paper and limited resources, the third strategy will be the central focus.

METHODS AND PROCEDURES

A complex statistical analysis would be most adept at determining the relationship between the factors identified above, which would typically be classified as dependent variables (adoption of cryptocurrencies) and independent variables (Western sanctions, economic volatility, resource curse, low GDP, and high levels of corruption). But, given the limited availability of data and the fact that the number of cases of state cryptocurrency adoption worldwide is under fifty countries, statistical analysis would not be feasible or even the best option. Instead, I will use Mill's method of agreement, where I will seek to determine if my independent variables of interest, or "attributes," lead to the outcome of cryptocurrency adoption, suggesting a possible correlation, if not outright causality.

The factors that lead a government to transition to blockchain technology and adopt cryptocurrency have not yet been determined. Blockchain is a revolutionary technology without precedent, therefore, making it challenging to assess historically. Thus, this study faced hurdles when researching transaction volume in governments and overall data in these countries. First, measuring corruption is a difficult task in itself. Next, cryptocurrency is an emerging field with limited publications; hence, specific sources currently published were included to ensure the credibility of this research. Such sources include peer-reviewed journals, projects, and government statistics. Also, the three case study countries have high levels of corruption, bribery, and lack of transparency, which may result in unreliable and tampered data. Finally, cryptocurrency and blockchain are more understood in finance and technology, as these concepts are commonly paired together, whereas this research encompasses an unprecedented perspective that focuses on political science and theory.

I have operationalized each attribute as follows. Higher levels of corruption may result in the adoption of native cryptocurrency. Hence, I quantified kleptocracy on an international scale. I used the Corruption Perception Index[12] to assess the three countries in this study. They were ranked on a scale from 0 to 100 based on public perception of corruption, with 0 being the most corrupt and 100 being the least corrupt. Additionally, I utilized the Economic Freedom Index[13] and Human Freedom Index[14], which operate on the same scale described above, to further measure kleptocracy. I measured Gross Domestic Product (GDP) using the World Bank[15] with the expectation that all three countries have lower GDPs than other developing countries due to high amounts of corruption. In this paper, I will examine economic growth in terms of GDP annual growth; hence, if the countries display negative percentages of growth, this will define lower levels of economic growth. Alongside GDP, I will examine hyperinflation as consumer prices rise more than 50% a month. When receiving data from the World Bank, if export revenue in natural resources, such as gas or petroleum, comprises over 50%, I classified the country as economically dependent on one main resource. Another critical component in my analysis is Western sanctions. Embargoes and sanctions on resource-rich countries limit trading interactions internationally, which accounts for a lower GDP. Thus, there is a potential relationship between Western sanctions and the depreciation of the domestic currency, which will be discussed below. After Western sanctions had been in place for a while, I measured if the domestic currency had gradually inflated, deflated, or remained the same. Table 1 summarizes attributes based on the literature review and the methods of measurement that will test for common attributes in case study countries.

Attributes	Definition	Measurement
Kleptocracy	Corrupt form of government that "rules by theft"	Economic Freedom, Human Freedom Index, Corruption Perception Index
Corruption	Misuse of power to fulfill individualistic goals to acquire greater power	Corruption Perception Index
GDP	Total value of goods produced annually	World Bank
Economic Volatility	Vulnerability to international fluctuations, possibly due to lack of economic diversification	Export revenue exceeding 50% classified as economically dependent, measuring depreciation of currency, and inflation
Western sanctions	The United States and European Union imposing economic sanctions: penalties imposed on the economy to produce the desired outcome	U.S. and E.U. sanctions on case study countries

Table 1. Main attributes based on literature review.

To best assess the realities that led to the adoption of cryptocurrencies in the three countries, I have conducted detailed case studies of each. I will present these case studies next, followed by a comparative study of the three based on the method of agreement.

COMPARATIVE CASE STUDY COUNTRIES

Case Study Selection

I sought to analyze why countries adopt cryptocurrencies since it seemed countries developing cryptocurrencies were resource-rich kleptocratic regimes. Three countries with well-known kleptocracies were chosen to analyze interest in cryptocurrencies. I selected countries currently undergoing development with limited research that could pose a potential threat to the United States hegemon: Iran, Russia, and Venezuela fit these criteria. These countries were selected due to their shared attributes, such as facing Western sanctions, hyperinflated currencies, and abundance in natural resources, all with corrupt regimes in power. This relates back to the idea that government adoption of cryptocurrencies can be either for inclusiveness or furthering corruption, which will further be explored through the case-study countries. Although other countries have adapted or supported state-backed cryptocurrency, such as Estonia, the three case-study countries were chosen to measure what attributes are more likely to result in government adoption of cryptocurrency. While there are other (more democratic, less corrupt) countries that have adopted cryptocurrencies (China, Estonia), the scope of my paper is limited by time and resources, and thus the focus on countries that share several attributes and some lack of variation in the selection of cases. I see the value in the inclusion of more varied cases in a future project. Hopefully, one will develop while completing graduate-level work.

The Islamic Republic of Iran

In Iran, clientelist relations and corruption have been affiliated with the high-ranking clerics of the Islamic Republic, who have access to innumerable political and economic privileges. The source of income is the rentier state and oil.[15] Oil is an abundant resource that has given Iran the opportunity to achieve vast amounts of wealth if managed wisely. However, Iran's natural resources are in the hands of the state and of its kleptocratic leaders.

In 2017, Iran's GDP growth dropped 3.8% due to dissipating oil prices and the effects of Western sanctions. According to the World Bank,[16] growth came from non-oil sectors, such as services (4.4%). Iran's GDP from 2018 and 2019 will be interesting to note due to the high influx of Western sanctions and travel bans intact.

Global relations open doors to international trade and greater wealth, and Iran's GDP could be impacted by the severance of Western ties. For these reasons, the government will have to devise strategic plans accordingly to circumvent the impact of sanctions. According to the 2019 Index of Economic Freedom,[13] Iran scored 51.1, ranking 155th freest in the world. Public debt is equivalent to 40% of the GDP. Investment freedom scored the lowest, revealing Iran has repressed opportunities to advance its economy through foreign direct investments. State-owned commercial banks and specialized financial institutions, appointed and reviewed by the Supreme Leader, account for most of the financial sector.

Iran is not part of the WTO, and Western sanctions decrease the openness of the Iranian economy[8] leading to less transparency and more opportunity for corruption.

In 2011, seven state-owned and private Iranian banks were involved in a $2.8 billion embezzlement case, possibly including forged documents. Subsequently, in 2014, there was another embezzlement scandal worth more than $4.5 billion from the Tejarat Bank. Scholars have found a positive relationship between the number of corruption cases and oil revenue – there was an $11 million increase in oil revenue from 1984 to 1989 and almost double the number of corruption cases during this time as well. Dadgar and Nazari[8] noted that Iran was ranked 138 out of 180 countries internationally.[17]

Before the Nuclear Deal was officially implemented in 2012, Iran endured sanctions on the Central Bank of Iran, importation of oil in seven major customer countries, and other economic sanctions. The United States was hoping sanctioning Iran could ultimately pressure the regime to forfeit any possibility of developing nuclear weapons. Consequently, economic sanctions and oil sanctions caused volatility in the exchange rate of Iran. The rial lost 80% of its value, and the reliance on the importation of goods led to increasing inflation rates.[18] According to the World Bank, Iran's inflation rate rose 19.6% from 2011 to 2013. Another impact of Western sanctions is blocked access to Society for Worldwide Interbank Financial Telecommunication (SWIFT) which is an internationally recognized identification code for banks around the world. Iran no longer has access to SWIFT and cannot pay for imports or receive payments for exports.[19]

The Supreme Leader of Iran has introduced a new concept to circumvent the hurdles of Western sanctions, known as Resistance Economy.[19] This plan was expected to help combat Western sanctions and keep Iran's economy afloat. To save the deflated currency, the regime is in the process of developing a native government-backed cryptocurrency.[20]
Because Iran lacks modernization in technology, medicine, and architecture, the country relies heavily on imported items which drives inflation rates higher, depreciating the value of the rial. If executed correctly, the Resistance Economy should alleviate the impact of threats issued by the West and help regenerate the economy. Adopting cryptocurrencies is another viable option for the regime. Given the series of imposed Western sanctions and efforts to improve the economy, Iran's adoption of cryptocurrency is permissible under Shari'ah law and, in fact, could bring a new era to the Middle East region.[20] The future of Iran's economy might hinge on the creation of native cryptocurrencies.

Iran is appealed to developing native cryptocurrencies in an effort to dodge brutal conditions the economy is enduring at a consequence of Western sanctions. The head of the Civil Defense Organization of Iran stated that "cryptocurrencies can help bypass certain sanctions through untraceable banking operations," clearly indicating Iran will privatize blockchain if transactions are "untraceable."[21] The adoption of cryptocurrencies will stabilize economic conditions by tokenizing the rial, facilitating trade in cross-border transactions, and bypassing Western sanctions. Iran has developed a native cryptocurrency, but the United States has passed the "Blocking Iran Illicit Finance Act," forbidding the use of digital currencies, like Venezuela in the preliminary stages of adopting the petro.[21]

Iran shows evidence of increased use of digital currencies among the population. Hadi Nemati, an Iranian cryptocurrency researcher, stated, "Bitcoin is a utility because it gives access to the world economy."[3] Iranians invest in Bitcoin because they have limited financial freedom and access to international fiat currencies. The population and government are seeking cryptocurrencies to skirt sanctions, which could pose a potential threat to the dollar.[3] With another round of sanctions, specifically targeting Iran's petroleum industry, the adoption of native cryptocurrencies remains a priority.

The Russian Federation
The economy in Russia made a gradual transformation from a centrally planned system into a market economy, its newly formed ruling oligarchy determined to capture the state's wealth, becoming a kleptocracy. The income inequality gap grew, shielded by weak legal and political institutions.[22]

Corruption is consistent in Russia, be it petty corruption, the bribing of low-ranking officials, or high-level corruption: large and illegal appropriation of state resources (privatization) by kleptocratic elites.[23]
Russia has an abundance of resource-rich commodities. Russia's natural gas extraction grew by 8.2% in 2017, accounting for over one-third of global growth. Russia's oil reserves rank 6th in the world and possess 18% of the largest gas reserves in the world, similar to Iran and Venezuela. In 2009, oil and natural gas accounted for 80% of the country's export. These attributes result in an economy volatile to global market fluctuations.

Recent Western sanctions have placed limitations on Russia's foreign policy ambitions and impacted its economy. The ruble depreciated by 50%, foreign direct investment has decreased by 5%, and oil prices have dropped 50%.[24] Devaluation of the ruble against the dollar has been caused by falling oil prices. Because Russia's economy depends on resources, Russia has developed a native government-backed cryptocurrency, known as the CryptoRuble, with an alternative version to blockchain called MasterChain to alleviate U.S. sanctions.[25]

A buffer layer is coded in MasterChain; any funds will be accessible to the Russian oligarchy and hidden from the Federal Reserve, United States Government, and the European Union. The development will grant Russia's monetary system independence from Western central banks' supervision. Hence, the CryptoRuble could effectively launder money through the Russian authorities and kleptocrats while escaping Western sanctions and privatizing the blockchain system.[25]

Russia's cryptocurrency would be backed by commodities such as gold and oil. President Putin's advisor, Sergi Glazyev, stated, "cryptocurrencies may help Russian banks avoid international sanctions" and supports the creation of a digital ruble.[3] Russia has utilized the functions of cryptocurrency mining, and Russian energy companies, such as Gazprom and EuroSibEnergo, recently declared they were negotiating the sale of 70 Bitcoin-mining companies.

The Bolivarian Republic of Venezuela
Venezuela is a petro-state with three interrelated attributes: export revenue is highest in natural resources, economic and political power is concentrated in the kleptocracy, and political institutions are weak and unaccountable, resulting in increased amounts of corruption.

Corruption permeates the political, social, and economic realm in Venezuela, with bureaucrats disregarding regulations and citizens paying bribes to compensate for the lack of basic government services.[26] According to the 2018 Transparency International Corruption Perception Index, Venezuela was ranked 168 out of 180 countries. Venezuela has an extensive history of political instability caused by mismanagement of resources, lack of transparency, and high amounts of corruption committed by the ruling elite – Maduro's administrative party.[6]

Oil constitutes 98% of Venezuela's exports, creating heavy dependence and high economic volatility.[27] Washington imposed sanctions targeting Venezuela's oil industry to deplete Maduro from obtaining a vital stream of income, leaving a profound effect on the economy.

Venezuela's cryptocurrency, known as the petro, is backed by oil, gold, gas, and diamond reserves[28] and is aimed at controlling the money supply and avoiding Western sanctions imposed by U.S. President Trump in 2017.

President Maduro stated that his "government would issue nearly $6 billion of petros as a way to raise hard currency and to evade financial sanctions imposed by Washington."[27] This development was accomplished with the assistance of Russia's cyber capabilities and speculated to be a practice-run of how the CryptoRuble would operate.[3] The petro's value has been pegged on the market price of oil and is backed by a "purchase-sale" contract. The petro is controlled by the Venezuelan Executive, making this the first state-backed national cryptocurrency.[28]

In efforts to fight hyperinflation, Maduro announced that the "Sovereign Bolivar" will have its value anchored to the petro. The Sovereign Bolivar is a new currency that eliminates five digits from the current currency, with the value linking to the petro.[28] The petro fluctuates in accordance, forming an interdependent relationship between these two currencies.

Another reason for cryptocurrency is to help alleviate debt. The petro serves as an instrument of financing for the Venezuelan government to issue debt to be traded among parties and accompanied by the illegal promise of an oil reserve guarantee. Looking deeper into the Presidential Decrees, it was discovered the petro was a creative tactic developed to address Venezuelan debt by using blockchain technology disguised as currency. [27] These oil reserves that were allegedly supposed to back the petro were "potential" and not yet developed. Therefore, the petro was sold at the price of the Venezuelan oil basket at the time but was illegitimately backed by nothing.[28] The main purpose of the petro was formed to relinquish the kleptocracy from exorbitant debt, whereas the Sovereign Bolivar aimed to control hyperinflation.

The petro is considered a variation of cryptocurrency; it was a promise from the Maduro regime that one petro could be traded for a physical oil barrel.[27] The Maduro administration mislead the population to create an illusion of stability, but with the ulterior motive of addressing debt. At best, the most beneficial aspect of the petro is trade. For example, the petro can trade goods or services, other cryptocurrencies, or pay the state with no interest rate.[28] If the state were to correctly execute this, the petro could have alleviated hyperinflation and provided a stronger economic base in Venezuela. However, given Venezuela's past of constant corruption with issuing debt and illicit drug trade, blockchain can also assist with strengthening Maduro's kleptocracy. If the distributed ledger is privatized, this will allow the government to fulfill its agenda of illicit trading and further corruption scandals. The illicit drug trade has been a constant epidemic, and governments may be lured into moving this operation onto a private blockchain to hide their transactions more effectively. Private blockchain only allows access to those invited, and transactions are anonymous. Thus, if governments continue their drug trade agenda, they can potentially succeed through the private blockchain. Venezuela is ranked the most corrupt country in this study and has officially adopted a native government-backed cryptocurrency on false pretenses.[6] Hence, this affirms the potential relationship between corruption and the adoption of native government-backed cryptocurrencies.

RESULTS

The shared attribute of depreciating currency is the most probable reason for prompt cryptocurrency adoption, alongside Western sanctions, which isolate economies, whereas cryptocurrencies offer a revolutionary system of backing currency through state commodities, uninfluenced by the dollar. The main finding of this paper includes a potential relationship between certain attributes and the rapid adoption of cryptocurrency, which calls for future statistical research, but this analysis provides a starting point by identifying shared attributes that might drive this shared outcome. Within the case study countries, Venezuela's findings demonstrate highly corrupt regimes (alongside other factors) are more likely to adopt native cryptocurrencies. However, in all three cases, it is worth noting that these governments are more prone to privatizing blockchains to enhance illicit activities. Iran, Russia, and Venezuela have expressed interest in various forms of illicit behavior, and because these countries are relatively corrupt in the global eye, a private blockchain can continue to fulfill such agendas.

Figure 1: There is a distinguishable pattern when measuring corruption, social, and economic freedom in the case study countries. Venezuela scored the highest in all three indexes, translating to high corruption with high amounts of social and economic repression. The Corruption Perception Index is measured out of 180 countries, and the value assigned correlates to how corrupt the country is; hence, the higher the number, the more corrupt a country is. The Economic Freedom Index is measured on a scale of the lowest number representing freedom. Hence, the lower the number, the more economically free that country is. Because Venezuela scored 177, this translates to a highly restrained or repressed economy. Finally, the Human Index measures freedom based on the higher the number, the less free a country is.

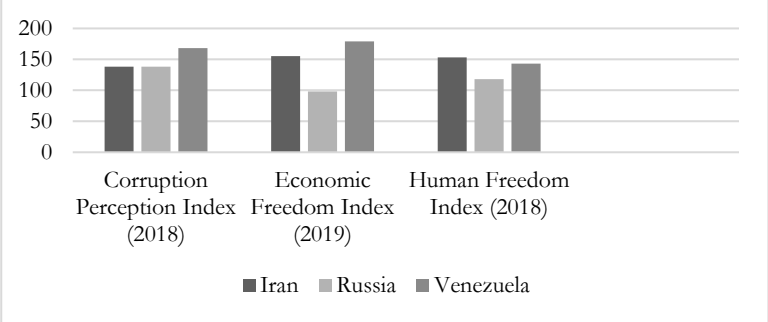

Figure 1. Corruption and freedom in Iran, Russia, and Venezuela Source: CPI (2018), EFI (2019), HFI (2018)

Iran and Venezuela had similar annual GDPs. According to the World Bank, in 2017,[15] Iran and Venezuela were in the bracket of $400,000 million, whereas Russia exceeded $1.5 trillion in annual GDP. However, further economic growth varies in these countries. Iran declined to 3.7% due to a shortage of oil export, Russia increased to 1.5%, and Venezuela scored -3.8%. Regardless of Venezuela's resemblance in GDP to Iran, the economy is rapidly shrinking and provides little economic growth, which explains the prompt adoption of cryptocurrency. Venezuela is suffering from a 254% consumer price inflation in 2016, labeling this as hyperinflation. Iran and Russia's economy experiences devalued currency with inflation, but insignificant compared to Venezuela. With Western-imposed sanctions, GDP growth is expected to fall and inflation rates to rise. According to the CIA Factbook,[27] 60% of export revenue is based on oil in Iran, and Russia scored similarly to this at 68%, while Venezuela's export revenue accounts for 98%.

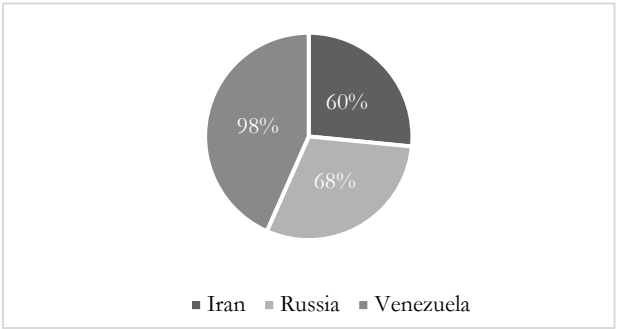

Figure 2. Crude Oil Export Revenue % (Source: CIA Factbook, Russia "B.P." (2018)).

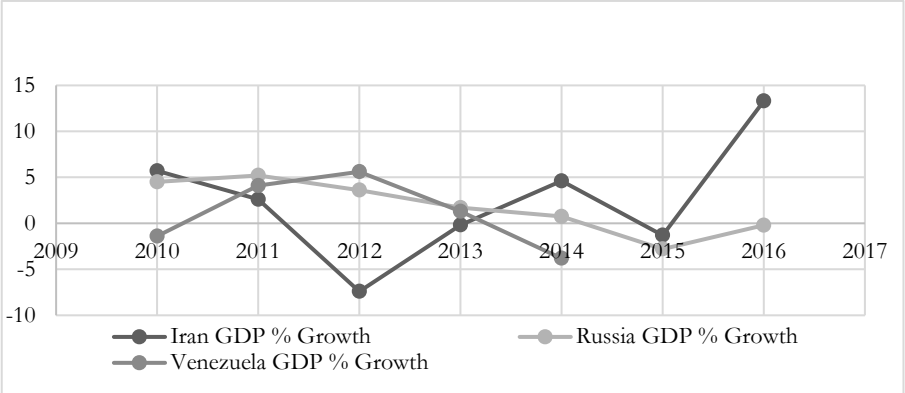

Figure 3: Iran, Russia, Venezuela GDP growth % (Source: World Bank).

Figure 2 shows the common attribute of economic dependence on crude oil, which may increase economic volatility in the market. In addition to oil, Iran and Russia's export revenue also depends heavily on natural gas.

Figure 3: This graph highlights the rise and decline of GDP growth according to the World Bank.[15] Iran's GDP growth declined to -7.4% in 2012 as the regime refused to comply with the nonnuclear proliferation agreement (the "Nuclear Deal"). In 2015, Russia's invasion of Crimea resulted in Western-imposed sanctions, which accounted for -2.8% GDP growth. Furthermore, Western sanctions on Russia were enforced until January 2019, causing economic backlash. In 2014, Western sanctions were imposed on Venezuela due to the humanitarian violations, thus, resulting in -3.8% GDP growth. While this decrease might be caused by other factors besides sanctions, the impact of international sanctions on GDP is well established in the literature in several other cases.[29; 30] After 2014, Venezuela's GDP was not recorded in the World Bank[15] and could not be graphed in Figure 1.7

Iran, Russia, and Venezuela have kleptocratic political systems that revolve around exploiting resource-rich capabilities and corruption for self-serving purposes. These kleptocrats have numerous characteristics in common, such as consolidating absolute power, committing election fraud to secure eternal reign, and inefficient state policies, amongst others.

The high deficit, depreciating currency, and inflation are the most significant factors that incentivize the adoption of cryptocurrencies. In 2013, the exchange rate between the Iranian rial to the dollar was fixed at 25,912 but dramatically increased to almost 33,000 in 2017, and currently, the rial has lost 80% of its value. In the wake of increased Western sanctions under President Trump, the rial is expected to depreciate continually.

Iran is now attempting to salvage the economy by utilizing its native cryptocurrency, even with the United States forbidding exchange. The case is similar in Russia and Venezuela. Russia's ruble has significantly depreciated, but President Putin's kleptocracy is developing CryptoRuble to alleviate economic pressures. Venezuela's poor economic policy, extreme hyperinflation, and high amounts of debt led President Maduro to adopt the petro. The population has adopted Bitcoin to informally pay for basic goods because the domestic currency is devalued, depreciated, and essentially worth very little.

Kleptocrats have passed various economic policies to relieve these conditions – Maduro raised the minimum wage five times, causing inflation, Ayatollah Khamenei's resistance economy plan, and Putin's expansion of the private sector, which increased corruption. Ineffective efforts to alleviate long-standing damages to their economies have backfired due to poor execution. Hence, the creation of a new national cryptocurrency backed by commodities is appealing. The similarities in the political and economic realms explain factors in agreement; highly corrupted statist economies run by kleptocrats, abundance of resources, limited economic growth, Western sanctions with increased inflation, and devalued currency. Iran, Russia, and Venezuela's socioeconomics resemble one another, which explains their shared interest in developing cryptocurrency.

Table 2 highlights the methods of agreement approach and outcome in case study countries: adoption of cryptocurrencies. The inputted number in corruption is based on the 2018 Corruption Perception Index.[12] GDP is primarily dependent on oil and natural gas, which can form an economically volatile country. While Iran and Russia experience growing levels of inflation and lower economic growth, Venezuela has severe economic conditions that likely pushed the Maduro administration towards the formal government adoption of a cryptocurrency immediately. In Iran, Western sanctions blocked the petroleum industry, pushing the regime to launch a native government-backed cryptocurrency.

	Iran	Russia	Venezuela
ATTRIBUTES:			
Corruption*	138	138	168
GDP Dependence on Natural Resources	✖	✖	✖
Inflation	✖	✖	✖
Low Economic Growth	✖	✖	✖
Economic Volatility	✖	✖	✖
Depreciated Currency	✖	✖	✖
Western Sanctions	✖	✖	✖

Table 2. Methods of agreement and outcome

Legend: X's indicate present factor

In comparison to the other countries, Venezuela has the greatest economic dependence on resources, is impacted severely by Western sanctions, hyperinflated currency, negative economic growth, and is ranked the most corrupt country. However, GDP is not as significant in determining the country's likelihood of adopting cryptocurrency, and the more important distinction lies in GDP growth. Lower levels of economic growth, such as growing inflation rates, devalued currency, and lack of diversification, can lead countries to resort to using cryptocurrencies.

Internationally, there has been growing interest in adopting native cryptocurrencies. In developing resource-rich countries with kleptocracies ruling, the intent for cryptocurrency culminates in efforts to expand power and exploitation. To some extent, Iran, Russia, and Venezuela's kleptocracies view cryptocurrency as a bargaining chip to threaten the hegemonic power of the United States. This is distinguishable in BRICS, a unification of sanctioned countries under one blockchain and currency due to a shared set of attributes or a common goal. These kleptocracies have aligned interests in consolidating more power and circumventing Western influence.

Blockchain can easily enhance corruption in every socioeconomic sector through illicit state monopolies that leave greater room for mismanagement of resources and, consequently, lower levels of economic growth. Alongside mismanagement, reliance on export revenue solely generated from resources; increases volatility and allows for potential instability in all three countries. Cryptocurrencies emerge as a potential solution to stabilize conditions politically and economically in kleptocratic countries while still granting innumerable rights to conduct corrupt behavior.

The goal of this paper was to analyze factors that may result in the adoption of native government-backed cryptocurrencies in three countries: Iran, Russia, and Venezuela. The findings of this research are notable: shared attributes common in each kleptocratic country; resource-rich capabilities that are heavily exploited, unstable economic conditions such as inflation, Western sanctions that limit international trade and raise inflation, high economic volatility due to lack of economic diversification, and increasing rates of corruption likely lead to the adoption of native cryptocurrencies, and illicit state behavior through a privatized blockchain.

ACKNOWLEDGEMENTS

Of all the people who have supported me in the fulfillment of my academic goal, there are four whom I acknowledge. First, my thesis chair, Dr. Anca Turcu, the most inspirational professor and advisor, challenged me in ways I never knew imaginable. Prior to writing this thesis, I was unaware of research design, and her unconditional patience and guidance were absolutely central to this project's completion. Her constructive criticism of my nebulous thoughts and often vague ideas helped form the foundations of this paper. I must also express my gratitude towards my committee member, Dr. Demet Mousseau, for teaching international economic principles that were applicable and incorporated in this paper. Her willingness to give time so generously was very much appreciated. I am eternally grateful for my family, who provided unconditional love and support. Thank you for encouraging my dreams and pursuit of happiness – the emotional and mental support was unparalleled. Finally, I wish to thank my colleagues who have aided the development of my scholarly pursuits.

REFERENCES

1. Acemoglu, D., Verdier, T., & Robinson, J. A. (2004) Kleptocracy and divide-and-rule: A model of personal rule. *Journal of the European Economic Association*, *2*(2-3), 162-192. *https://doi.org/10.1162/154247604323067916*
2. Appelbaum, D., & Stein Smith, S. (2018) Blockchain Basics and Hands-on Guidance: Taking the Next Step toward Implementation and Adoption. CPA Journal, 88(6), 28-37.
3. Konowicz, D. R. (2018) The New Game: Cryptocurrency Challenges U.S. Economic Sanctions. Naval War College Newport United States
4. BUTTON, S. (2018) Cryptocurrency and Blockchains in Emerging Economies. Software Quality Professional, 20(3), 39-46
5. V Rindborg, G. (2018) Venezuelan Oil and Political Instability: A Case Study of Venezuela and its Oil Dependency. Stockholm University, Faculty of Social Sciences, Department of Sociology. *Oai:DiVA.org:su-156457*
6. Hirschkorn, J., Levanov, A., Titov, A., & Williams, R. Nation-State Adoption of Distributed Ledger Technology: (2018) How Blockchain Will Remake Traditional Nation-State Relationships. *The Stanford US-Russia Forum Research Journal* (Vol. 9, p. 37).
7. Tanzi, T. (2013) Corruption and the Economy. Filozofija I Drustvo, 24(1), 33-59. *https://doi.org/10.2298/FID1201033T*
8. Dadgar, Y., & Nazari, R. (2012) The impact of oil revenue on the economic corruption in Iran. Актуальні проблеми економіки, (2), 375-386
9. Viglione, R. (2015) Does Governance Have a Role in Pricing? *Cross-Country Evidence from Bitcoin Markets. http://dx/doi.org/10.2139/ssrn.2666243*
10. Galı, J., & Gertler, M. (1999) Inflation dynamics: A structural econometric analysis. Journal of monetary Economics, 44(2), 195-222. *https://doi.org/10.1016/S0304-3932(99)00023-9*

11. Samimi, A. J., & Jamshidbaygi, S. (2011) Budget deficit and inflation: A sensitivity analysis to inflation and money supply in Iran. *Middle-east Journal of scientific research*, 8(1), 257-260.
12. E.V., T. I. (n.d.) Corruption Perceptions Index 2018, *https://www.transparency.org/cpi2018* (accessed April 2019)
13. 2019 Index of Economic Freedom. (n.d.), *https://www.heritage.org/index/*(accessed April 2019)
14. Human Freedom Index. (2018) *https://www.cato.org/human-freedom-index-nex* (accessed April 2019)
15. Cuevas, M. A. (2002) Potential GDP growth in Venezuela: A structural time series approach. The World Bank.
16. Alamdari, K. (2005) The Power Structure of the Islamic Republic of Iran: transition from populism to clientelism, and militarization of the government. Third World Quarterly, 26(8), 1285-1301. *https://doi.org/10.1080/01436590500336690*
17. "Transparency Index – the Most Transparent Companies." *Transparency Invest, transperancy.com/transpernacy.index/*
18. Rahmani, T., & Koohshahi, N. M. (2015) Legal Analysis of Procurement Corruption in Iran Economy. International Journal of Management, Accounting & Economics, 2(12), 1484-1496.
19. Babak, A. (2013) Threat of Sanctions and Management of Resistance Economy in Iran. American Journal of Scientific Research, (86), 111-116.
20. Oziev, G., & Yandiev, M. (2017) Cryptocurrency from Shari'ah Perspective. (n.d.). Nicolás Maduro, *https://www.occrp.org/personoftheyear/2016/* (accessed April 2019).
21. Blocking of Iran Illicit Finance Act of 2018, H.R. 7321, 115d Cong., 2nd Sess. (2018)
22. Yakovlev, E., & Zhuravskaya, E. (2009) State capture: from Yeltsin to Putin. *In Corruption, Development and Institutional Design* (pp. 24-36). Palgrave Macmillan, London. *https://doi.org/10.1057/9780230242173_2*
23. Russia. (n.d.) *https://www.bp.com/en/global/corporate/energy-economics/statistical-review-of-world-energy/country-and-regional-insights/russia.html*
24. Nelson, R. M. (2015) U.S. Sanctions on Russia: Economic Implications. Washington, DC: Congressional Research Service.
25. Kakushadze, Z., & Liew, J. K. S. (2018) CryptoRuble: From Russia with Love. arXiv preprint. *https://doi.org/10.48550/arXiv.1801.05760.*
26. Coronel, G. (2006) Corruption, mismanagement, and abuse of power in Hugo Chávez's Venezuela (Vol. 2). Cato Institute Center for Global Liberty & Prosperity.
27. The World Factbook: IRAN. (2018) https://www.cia.gov/library/publications/the-world-factbook/geos/ir.html (Links to an external site.) Links to an external site & The World Factbook: RUSSIA. (2018) *https://www.cia.gov/library/publications/the-world-factbook/geos/rs.html* & The World Factbook: VENEZUELA. *https://www.cia.gov/library/publications/the-world-factbook/geos/ve.html* (accessed Oct 2018).
28. Herrera Anchustegui, Ignacio and Hunter, Tina, Oil as Currency: Venezuela's Petro, a New 'Oil Pattern'? (2018) Available at SSRN: *https://ssrn.com/abstract=3291272 or http://dx.doi.org/10.2139/ssrn.3291272*
29. Neumeier, F., & Neuenkirch, M. (2014) *The Impact of UN and US Economic Sanctions on GDP Growth* (No. 201424) Philipps-Universität Marburg, Faculty of Business Administration and Economics, Department of Economics (Volkswirtschaftliche Abteilung). *https://doi.org/10.1016/j.ejpoleco.2015.09.001*
30. Shirov, A. A., Yantovskii, A. A., & Potapenko, V. V. (2015) Evaluation of the potential effect of sanctions on the economic development of Russia and the European Union. *Studies on Russian Economic Development*, *26*(4), 317-326. *https://doi.org/10.1134/S1075700715040103*

ABOUT STUDENT AUTHOR

Rose Mahdavieh is a recent graduate from the University of Central Florida, with a B.A. in Political Science and a minor in Intelligence and National Security. This research was conducted and published in her undergraduate honors thesis, which received a nomination for a scholarly award as one of the most downloaded theses in the Department of Political Science. Rose will continue to law school and pursue blockchain and international law.

PRESS SUMMARY

Advancements in technology are influencing and shaping international politics in an unprecedented era of changing times. This article analyzes the new trend of digital currency being cutting-edge and the application of governments adopting such technology. While digital currency transforms the political and financial realm, a select few governments are privatizing cryptocurrencies and blockchains to further break international law or threaten security of nations. In studying specific attributes these governments share, their conduct is more discernable, and international powers can conglomerate to prevent further corruption.

Salinity Affects Wound Healing in Wild Common Bottlenose Dolphins (*Tursiops truncatus*)

Brianna Hurst & Dara N. Orbach*

Department of Life Sciences, Texas A&M University-Corpus Christi, Corpus Christi, TX

https://doi.org/10.33697/ajur.2022.056

*Student: bhurst2@islander.tamucc.edu**
Mentor: dara.orbach@tamucc.edu

ABSTRACT
Dolphins are often individually identified by unique naturally-acquired markings. Identification becomes difficult when markings heal, or new scars appear. As salt accelerates wound healing in many organisms, the diminishment of scars on common bottlenose dolphins (*Tursiops truncatus*) residing in varying natural salinities was determined. South Texas contains the only hypersaline lagoon in the USA, located adjacent to hyposaline waters, with genetically distinct populations of dolphins in the two environments. Photographs of dolphin dorsal fins were collected, and scar stability over time was determined and compared by measuring changes in the relative lengths and surfaces of scars. All scars on dolphins in the hypersaline lagoon completely diminished between three to six years, while scars on dolphins in the hyposaline bay ranged in the amount of fading between three to six years. Data from this case study indicate that high salinity may increase the healing speed of wounds on common bottlenose dolphins compared to low salinity, although a larger sample size is needed for robust statistical comparison. Scar diminishment is an important consideration in determining the temporal reliability of photo identification.

KEYWORDS
Bottlenose dolphin; Corpus Christi Bay; healing; hypersaline; Laguna Madre; photo-identification; salinity; scar

INTRODUCTION

Photo-identification, in which animals are identified by individually distinctive markings, pigmentations, notches, or scars captured by cameras, is the most commonly used approach to determine the population abundance, habitat use, behavior, and impacts of human disturbance on cetaceans (whales, dolphins, and porpoises).[1–5] Small nicks may be acquired through a natural tattering of the dorsal fin, while larger nicks (termed notches) and wounds may be caused by interactions with predators, boats, fishing gear, or conspecifics, among other sources.[3] Nicks/notches on the dorsal fin are considered reliable for individual identification of many species of dolphins because of their visibility from each side of the animal in varied lighting conditions.[4,5] In contrast, a scar is only present on one side of the animal and may diminish over time. As markings may change naturally, either through healing or acquisition of new markings, consistent identification of individuals may have inherent limitations.[1] For example, pigment spots and bite marks usually persist for six months to one year in common bottlenose dolphins (*Tursiops truncatus*).[6] Changes in markings could skew data if an individual is misidentified, yet few studies have explored the long-term stability of wounds among cetaceans. Determining how long scars remain visible could provide a metric of the reliability of photo identification in changing environmental conditions (*e.g.,* hurricanes, climate change, freshwater run-off).

Measurements of the distance between notches on the dorsal fins of dolphins are a benchmark in re-sighting individuals using photo-identification[7] and are the basis of several semi-automated fin-matching software (*e.g.,* finFindR, Finbase, Finscan). However, there is no standardized technique to quantify scar characteristics on the dorsal fins of cetaceans. Research on scars has focused on identifying and categorizing potential sources.[3,4] Small surface wounds, such as tooth rake marks, generally heal faster than large or deep wounds caused by shark bites,[6] but the conditions of the water may affect the healing process. Thus, observations collected from free-ranging dolphins are potentially valuable for tracking natural wound healing.

The duration that scars persist may vary with salinity. Saline-treated wounds re-epithelialized (covered with tissue) faster than wounds treated in a dry or moist environment among porcine (pigs)[8] and showed less necrosis, inflammation, and scar formation.[9] In humans and mice, cutaneous salt storage boosts the activation of macrophages, facilitates pathogen removal, and aids in combating bacterial infections.[10] Epidermal changes associated with low salinity exposure (0-30 ppt) were recorded in common bottlenose dolphins.[11] An uptake of low saline water from the environment suggests low blood sodium, blood chloride

ion, and extracellular plasma sodium concentrations.[12] Of the few studies that have explored wounds of dolphins under extreme salinity conditions, only the effects of low salinities have been assessed.

There are few locations globally with naturally high salinity levels above standard seawater (35 ppt) conducive to assessing long-term healing patterns without manipulating environmental conditions. The Laguna Madre, TX, is the only hypersaline lagoon in the USA, with an average salinity of 36 ppt that has periodically doubled the Gulf of Mexico.[13] The Laguna Madre extends from Corpus Christi south to Port Isabel, TX, and consists primarily of seagrass beds.[13] Laguna Madre is inhabited by a stock of common bottlenose dolphins that is genetically distinct from the adjacent Corpus Christi/Redfish Bay population, which are both genetically distinct from dolphins inhabiting the Gulf of Mexico.[13] Corpus Christi/Redfish Bay is often hypoosmotic (average salinities 22-27 ppt).[13] The South Texas coastline provides a unique opportunity to compare how varying natural salinity levels affect the temporal stability of wounds on common bottlenose dolphin dorsal fins. We present a case study on bottlenose dolphin wound healing in South Texas. It was hypothesized that wound healing would vary significantly between the two locations, with Laguna Madre dolphins predicted to heal more than Corpus Christi/Redfish Bay dolphins.

METHODS AND PROCEDURES

Photographs of common bottlenose dolphin dorsal fins were captured between 2014 and 2020 during boat-based surveys along the Corpus Christi/Redfish Bay and Laguna Madre, TX, coastline. Data were collected under NOAA NMFS permit numbers 18715, 18881, and 23203. Dolphin group sizes, GPS coordinates, salinity levels, and weather conditions were recorded for each group encountered after photographs were collected with a Nikon D3200 or Nikon D7000 camera with 70-300mm or 80-400mm Nikkor lens. Dolphin groups were defined as individuals swimming within 10m and exhibiting the same behavior state.[14] GPS coordinates were recorded with a Garmin GPS map 540s, Lowrance HDS7, or Lowrance HDS5, and salinity levels were recorded with a YSI Pro 20. Upon visually spotting dolphins, the research boat (17ft Carolina Skiff DLX, 23ft Stoner Supercat, or 18ft Inmar 550R-DR) traveled towards the dolphins in a parallel heading at low speed. Dolphins were observed for under 30 minutes, and follows were terminated if dolphins were evasive. Surveys were only conducted during daylight hours in weather conditions deemed safe for small boats (*e.g.*, low winds, no fog, Beaufort Sea State < 3).

A digital catalog of dolphin dorsal fin photographs was established with metadata associated with each image. Photographs of fins were cropped, quality control-checked (in focus, not obstructed, not submerged, distinguishable features present)[5] and matched for re-sightings by interns at Texas A&M University-Corpus Christi. Fins were matched using FinFindR,[15], a semi-automated dorsal fin matching software, and verified by two researchers. Fins were matched within and across locations (Laguna Madre and Corpus Christi/Redfish Bay). Data were constrained to include dolphins with a minimum of two photographs collected three to six years apart, in which the same side of the dorsal fin (left or right) was photographed.

Wound healing was determined by measuring scars on dorsal fin photographs in ImageJ[16] using two new techniques:

1) *Relative scar length*: Photographs were adjusted in brightness and contrast to highlight scars. To standardize measurements, the length of the dorsal fin was measured using the 'Straight-line' tool in ImageJ from the most distal tip down the midline of the fin to its base (**Figure 1**); this fin length was calibrated to a scale of 1. The lengths of each scar were subsequently measured and tallied per photograph to calculate the sum of scars. Measurements of the same scars (visible in 'old' photographs) were collected for both 'old' photographs (2014-2017) and 'new' photographs (2020). The percentage change of scars per individual was derived as

$$\frac{\sum old\ photo\ scars - \sum new\ photo\ scars}{\sum old\ photo\ scars} * 100 \qquad \textbf{Equation 1.}$$

2) *Relative scar surface*: Photographs were adjusted for brightness and contrast to highlight scars. To standardize measurements, the one-dimensional surface of the dorsal fin was measured with the 'Freehand Selections' tool in ImageJ and calibrated to a scale of 1. Surfaces were traced using a Surface Pro 7 tablet. Each scar was subsequently outlined, and its surface was measured. Scar surfaces were tallied per photograph to calculate the sum (**Figure 2**). Measurements were converted to a ratio:

$$\frac{\sum scars}{surface\ of\ dorsal\ fin} * \frac{x}{1} \qquad \textbf{Equation 2.}$$

Measurements of the same scars were collected for both 'old' photographs (2014-2017) and 'new' photographs (2020). The percentage change of scars per individual was derived using **Equation 1.**

A t-test[17] was performed to determine if the percent wound healing differed significantly between the two locations with varying natural salinity levels. Qualitative patterns were assessed by plotting the straight length scarring ratios and corresponding salinity levels when each photograph was taken.

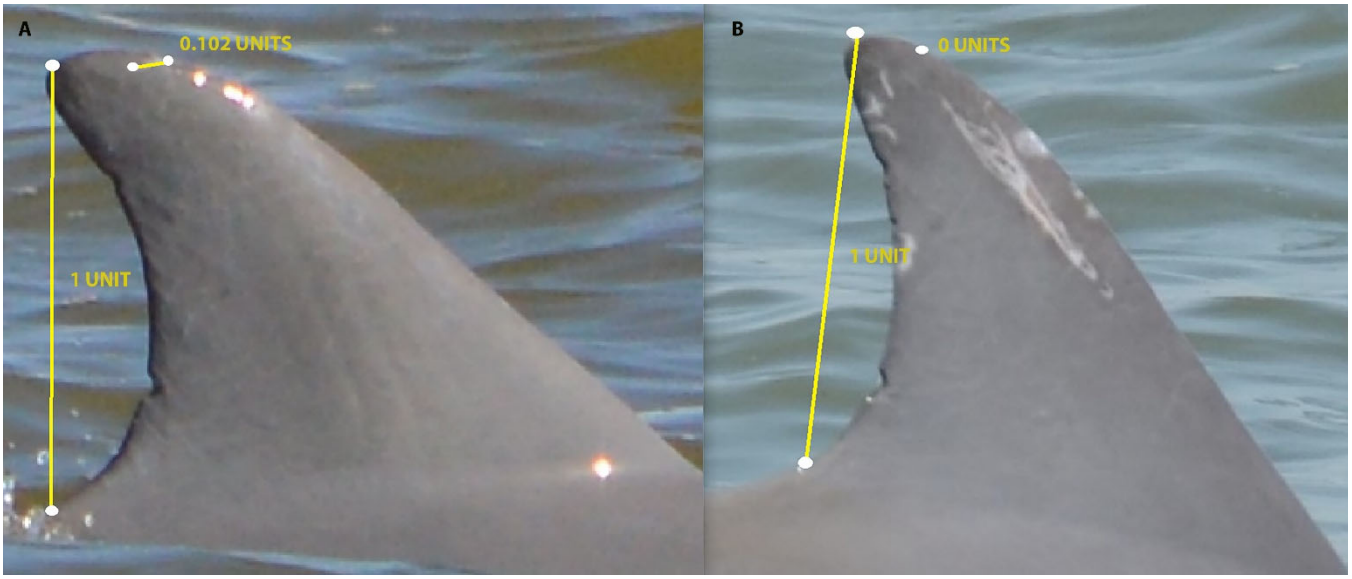

Figure 1: The dorsal fin of one common bottlenose dolphin captured five years apart: A) 'Old' photograph captured December 2015, B) 'New' photograph captured September 2020. White dots indicate the start and endpoints of landmarks. Relative units of measurement are listed. Only scars present in the 'old' photograph were analyzed.

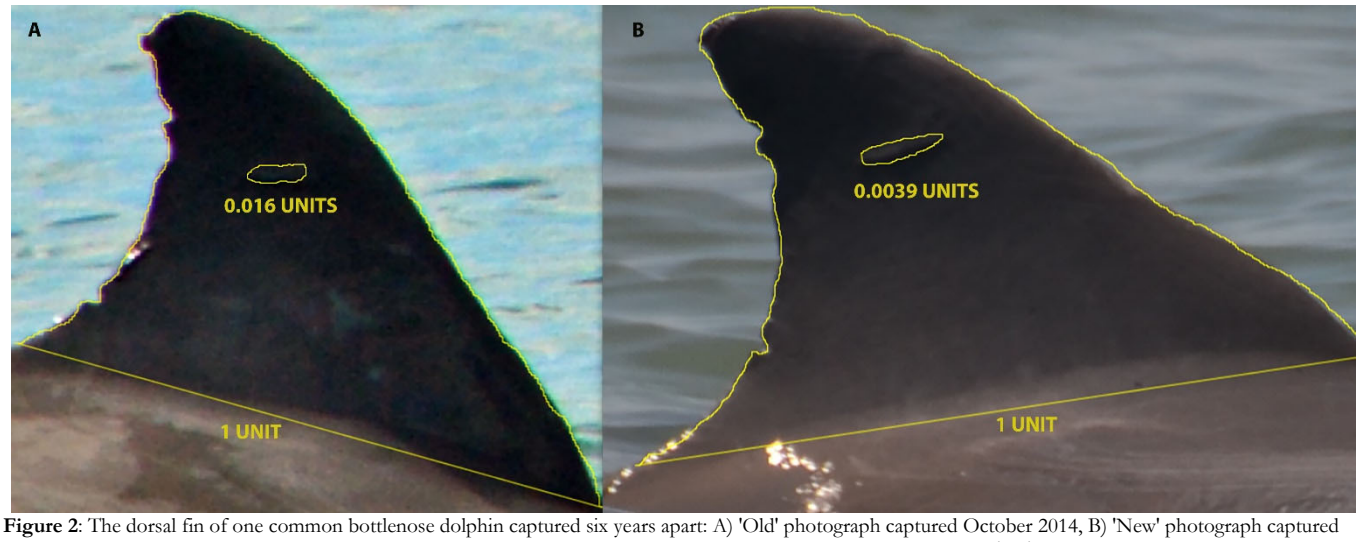

Figure 2: The dorsal fin of one common bottlenose dolphin captured six years apart: A) 'Old' photograph captured October 2014, B) 'New' photograph captured June 2020. Yellow outlines denote surfaces. Relative units of measurement are listed. Only scars present in the 'old' photograph were analyzed.

RESULTS

Between 2014 and 2020, four individuals were re-sighted at least three years apart in Laguna Madre and seven individuals in Corpus Christi/Redfish Bay. Within Corpus Christi/Redfish Bay, one individual was re-sighted on both sides of its dorsal fin during different surveys; each side of the dorsal fin was evaluated independently. LM1 and LM2 (September 2020) and LM3 and LM4 (November 2020) were re-sighted in the same group, respectively, while no other dolphins were initially or subsequently observed in the same group (**Table 1**). There was a 100% change in the length of scars observed within Laguna Madre data; no 'old' photograph scars could be detected in the 'new' photographs (**Figure 3**). In Corpus Christi/Redfish Bay, there was a range of percent changes in relative scar lengths (**Figure 3**). No significant difference was found in the amount of change in relative scar lengths (t= 1.267; p= 0.234) nor relative scar surfaces (t= 1.273; p= 0.232) between populations. Both length and surface measurements yielded similar patterns, with neither technique reliably producing higher values (**Table 1**). Within Laguna Madre, but not Corpus Christi/Redfish Bay, salinity levels were consistently higher when dolphins were re-sighted compared to the initial sighting (**Figure 4**; **Table 1**).

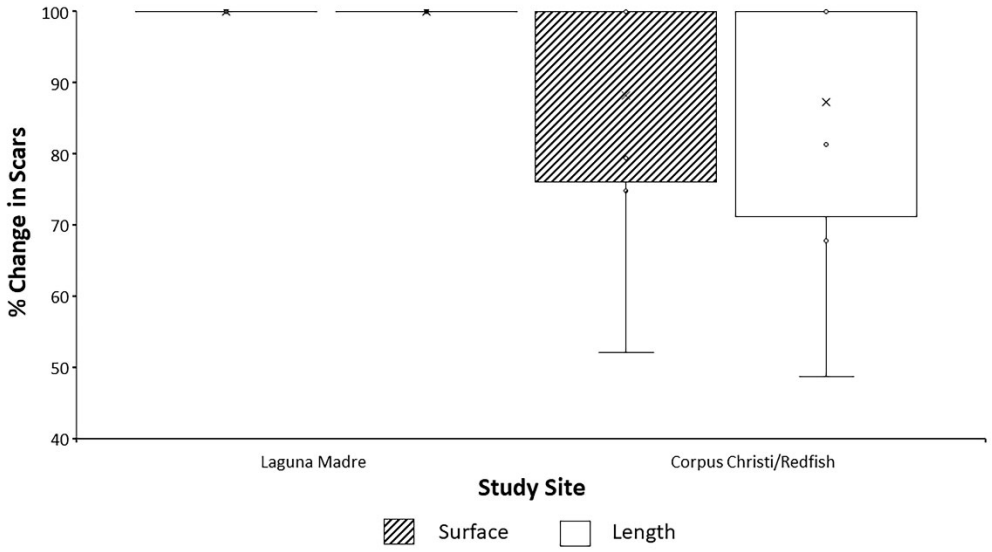

Figure 3: The percent change in cumulative scars for Laguna Madre and Corpus Christi/Redfish Bay populations of dolphins using length and surface measurement techniques. In these box-and-whisker plots, the 'x' represents the mean, and the 'whiskers' depict the maximum and minimum values.

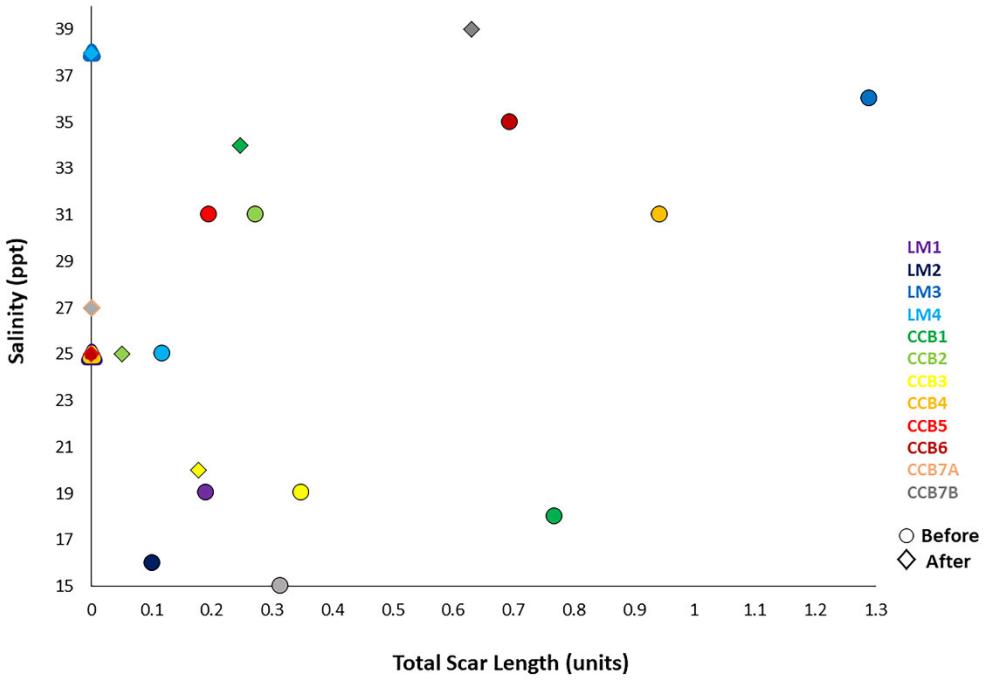

Figure 4: The total relative length of scars on common bottlenose dolphins at different salinities with the 'old' photograph delineated with a circle and the 'new' photograph delineated with a diamond. Each dolphin is designated by a different color. Symbols with multiple colors indicate more than one identical data point.

Individual	Site	Date-Old Photo	Salinity-Old Photo	Date-New Photo	Salinity-New Photo	% Change Linear Method	% Change Surface Area Method
LM1	Laguna Madre	December 2015	19	September 2020	25	100	100
LM2	Laguna Madre	December 2015	16	September 2020	25	100	100
LM3	Laguna Madre	November 2015	36	November 2020	38	100	100
LM4	Laguna Madre	December 2015	25	November 2020	38	100	100
CCB1	Corpus Christi Bay	April 2017	18	June 2020	34	67.88	52.18
CCB2	Corpus Christi Bay	April 2014	31	June 2020	25	81.32	79.46
CCB3	Corpus Christi Bay	October 2014	19	June 2020	20	48.85	74.89
CCB4	Corpus Christi Bay	April 2015	31	August 2020	25	100	100
CCB5	Corpus Christi Bay	April 2015	31	June 2020	25	100	100
CCB6	Corpus Christi Bay	April 2015	35	June 2020	25	100	100
CCB7A	Corpus Christi Bay	February 2017	39	September 2020	27	100	100
CCB7B	Corpus Christi Bay	February 2017	15	September 2020	27	100	100

Table 1. The site location, date, salinity, and percent change in scarring for each common bottlenose dolphin.

DISCUSSION

Our case study provides preliminary data suggesting that high salinities may diminish the scars of common bottlenose dolphins faster than low salinities. Dolphins residing in a hypersaline environment (Laguna Madre) showed a greater amount of scar reduction compared to dolphins in a hyposaline environment (Corpus Christi/Redfish Bay) over three to six years, as predicted, although this pattern was not statistically significant. All dolphins analyzed from Laguna Madre experienced 100% diminishment in scars over time, unlike dolphins from Corpus Christi/Redfish Bay. Dolphins in Laguna Madre were consistently re-sighted in elevated salinities (although initial salinities could sometimes not be hypersaline), whereas dolphins in Corpus Christi/Redfish Bay were re-sighted in variable salinities. As dolphins in Laguna Madre were generally not sighted in the same groups, and as dolphins in Corpus Christi/Redfish Bay were never observed in the same groups, both populations may have fission-fusion societies where individuals inhabit different parts of their ecosystem and are exposed to different salinities at any given time. It is unclear why patterns differed for CCB 1-3 compared to CCB 4-7, although the individuals in Corpus Christi that retained scars for at least three years (CCB1-3) appeared to have comparatively deep wounds that take longer to heal than shallow wounds in a low saline environment. This pattern may explain the range of error bars observed. Accordingly, it appears that salinity may be important in wound healing as found in other species.[8-10] As Laguna Madre experiences little water turnover due to its shallow depth and connection to few contributing sources of water, fluctuations in the salinity observed in the Laguna Madre may reflect recent rain events that increased freshwater inflow and lowered salinity.[18] A larger sample size is needed to determine if the observed trends are robust as statistics may not be biologically meaningful for a small sample size. Additional environmental parameters like water temperature, contaminate load, and pH could be tested as confounding variables in future studies.

New methods were implemented to measure scars. Both linear and surface measurements yielded similar scar diminishing patterns, suggesting comparable accuracy. A suite of measurements is recommended to standardize assessments of scar patterns on dolphins, including alternative metrics. Affine-invariant grids have been proposed to measure identifiable markings on humpback whales (*Megaptera novaeangliae*).[19] Melanistic leopards (*Panthera pardus*) have been reliably identified using infrared wavelengths to illuminate pigmentations of rosettes.[20] In humans, scar healing has been monitored using stimulated infrared thermography, where scars appear colder than peri-scar areas.[21] Stimulated infrared thermography presents a novel way to follow the progress of treatment for a scar[22] and may be applicable for marine mammals if limitations imposed by temperature, water opacity, and environmental factors can be overcome. Dorsal fins can act as thermal windows in infrared thermography.[23]
The ability to re-sight a dolphin will vary with wound, scar, and other identifying marks that may change over time. Studies using photo-identification may have varying reliability. Understanding the prevalence, longevity, reliability, and rate of change in markings used to identify individuals are critical as cetacean population studies primarily use long-term photo-identification data.[24] Epithelium repair occurs rapidly in bottlenose dolphins because of the exposed dermal papillae of the wound and extensive folding of the germinal layer.[6] Epidermal sloughing (shedding) is estimated to be 8.5x faster than in humans, occurring 12x daily in bottlenose dolphins;[25]; however, rates of sloughing may fluctuate with hormonal influence, diurnal effects, temperature, salinity, and response to trauma.[25] Constant and gentle irrigation of a wound in water may accelerate tissue repair.[6]

The duration between re-sighting dolphins likely greatly impacts scar diminishment. Three to six years between sightings appears to be too long to reliably assess the speed of wound healing. Instead, one year between sightings is recommended for common bottlenose dolphins, as small wounds such as bite marks and pigment spots usually heal annually.[6] Recommended durations are species-specific. For example, protruding fat marks can persist for six years, and scrapes can last several decades in Risso's dolphins (*Grampus griseus*).[26] Scars were unreliable for individual identification across years in northern bottlenose whales

(*Hyperoodon ampullatus*) compared to notches and back indents that had reduced rates of loss.[24] Additional research on small, closed populations of dolphins in which frequent re-sightings are possible can expand the scope of this case study and allow for fine-tuned quantification of the duration for scars to diminish entirely.

CONCLUSION

Data from this case study provide preliminary evidence that salinity may affect the diminishment of scars in bottlenose dolphins, although a larger sample size is needed for robust statistical analysis. As dolphins do not typically reside in hypersaline waters, Laguna Madre provided a unique environment to address questions about natural wound healing. We developed two novel metrics to quantify scars that may be widely applied to other cetacean species or marine fauna. Future studies may be able to apply these metrics in determining sources of scars. The development of additional metrics of scar size and rates of change are warranted for cetaceans as markings are prevalently used for population estimates despite evidence that scars do not appear to be stable over long durations.[23]

ACKNOWLEDGMENTS

The authors thank Will McGlaun (Texas Sealife Center) for photographs and data, Xavier Gonzales for lending a Surface Pro 7, and Anabel Hernandez and members of the Functional Anatomy and Behavioral Ecology of Marine Mammals lab at TAMU-CC for feedback and support. Funding was provided by the McNair Scholars Program at Texas A&M University-Corpus Christi.

REFERENCES

1. Auger-Methe, M., and Whitehead, H. (2007) The use of natural markings in studies of long-finned pilot whales, *Mar Mamm Sci23*(1), 77–93. *http://doi.org/10.1111/j.1748-7692.2006.00090.x*

2. Elwen, S. H., and Leeney R. H. (2010) Injury and subsequent healing of a propeller strike injury to a Heaviside's dolphin (*Cephalorhynchus heavisidii*), *Aqua Mamm 36*(4), 382–387. *http://doi.org/10.1578/AM.36.4.2010.382*

3. Kügler, A., and Orbach, D. (2014) Sources of notch and scar patterns on the dorsal fins of dusky dolphins (*Lagenorhynchus obscurus*), *Aqua Mamm 40*(3), 260–273. *http://doi.org/10.1578/AM.40.3.2014.260*

4. Luksenburg, J. A. (2014) Prevalence of external injuries in small cetaceans in Aruban waters, Southern Caribbean, *PLoS ONE 9*(2), 1–10. *http://doi.org/10.1371/ journal.pone.0088988*

5. Markowitz, T. M., Harlin, A. D., and Würsig, B. (2003) Digital photography improves efficiency of individual dolphin identification, *Mar Mamm Sci 19*(1), 217–223. *http://doi.org/10.1111/j.1748-7692.2003.tb01103.x*

6. Corkeron, P. J., Morris, R. J., and Bryden, M. M. (1987) A note on healing of large wounds in bottlenose dolphins, *Tursiops truncates, Aqua Mamm 13*(3), 96–98.

7. Defran, R. H., Shultz, G. M., and Weller, D. W. (1990) A technique for the photographic identification and cataloging of dorsal fins of the bottlenose dolphin (*Tursiops truncatus*), *Reports of the Intl Whaling Cmsn (Special Issue 12), 53–55*. SC/A88/P16.

8. Svensjö, T., Pomahac, B., Yao, F., Slama, J., and Eriksson, E. (2000) Accelerated healing of full-thickness skin wounds in a wet environment, *Plast Reconstr Surg 106*(3), 602–612. PMID: 10987467

9. Breuing, K., Eriksson, E., Liu, P., and Miller, D. (1992) Healing of partial thickness porcine skin wounds in a liquid environment, *JSR 52*(1), 50–58. *http://doi.org/10.1016/0022-4804(92)90278-8*

10. Jantsch, J., Schatz, V., Friedrich, D., Schröder, A., Kopp, C., Siegert, I., Maronna, A., Wendelborn, D., Linz, P., Binger, K. J., Gebhardt, M., Heinig, M., Neubert, P., Fischer, F., Teufel, S., David, J.-P., Neufert, C., Cavallaro, A., Rakova, N., Küper, C., Beck, F-X., Neuhofer, W., Muller, D. N., Schuler, G., Uder, M., Bogdan, C. Luft, F. C., and Titze, J. (2015) Cutaneous Na+ storage strengthens the antimicrobial barrier function of the skin and boosts macrophage-driven host defense, *Cell Metabolism 21*(3), 493–501. *http://doi.org/10.1016/j.cmet.2015.02.003*

11. McClain, A. M., Daniels, R., Gomez, F. M., Ridgway, S. H., Takeshita, R., Jensen, E. D., and Smith, C. R. (2020) Physiological effects of low salinity exposure on bottlenose dolphins (*Tursiops truncatus*), *J. Zool. Bot. Gard. 1*, 61–75. *http://doi.org/10.3390/jzbg1010005*

12. Ewing, R. Y., Mase-Guthrie, B., McFee, W., Townsend, F., Manire, C. A., Walsh, M., Borkowski, R., Bossart, G. D., and Schaefer, A. M. (2017) Evaluation of serum for pathophysiological effects of prolonged low salinity water exposure in displaced bottlenose dolphins (*Tursiops truncatus*), *Front. Vet. Sci. 4*(80), 1–7. *http://doi.org/10.3389/fvets.2017.00080*

13. Philips, N. M., and Rosel, P. E. (2014) A Method for prioritizing research on common bottlenose dolphin stocks through evaluating threats and data availability: Development and application to bay, sound and estuary stocks in Texas, *NOAA Tech Memo NMFS-SEFSC-665*. *http://doi.org/10.7289/V5F769H8*

14. Smolker, R. A., Ricards, A. F., Connor, R. C., and Pepper, J. W. (1992) Sex differences in patterns of association among Indian Ocean bottlenose dolphins, *Behaviour 123*(1), 38–69. *http://doi.org/10.1163/156853992X00101*

15. FinFindR v.0.1.6. (2019) Retrieved from *https://github.com/haimeh/finFind*R/*releases/tag/0.1.6*

16. Rasband, W. S. (2018) ImageJ, U. S. National Institutes of Health, Bethesda, Maryland, USA*, https://imagej.nih.gov/ij/*, 1997–2018
17. Social Science Statistics, T-Test Calculator for 2 Independent Means, *https://www.socscistatistics.com/tests/studentttest/default2.aspx*
18. Schoenbaechler, C., Guthrie C. G., Matsumoto, J., and Lu, Q. (2011). TxBLEND model calibration and validation for the Laguna Madre Estuary, *Texas Water Development Board*, 60pp.
19. Ranguelova, E. and Pauwels, E. (2005) Saliency detection and matching strategy for photo-identification of humpback whales, GVIP 05 Conference, *https://ir.cwi.nl/pub/14214*
20. Hedges, L., Lam, W. Y., Campros-Arceiz, A., Rayan, D. M., Laurance, W. F., Latham, C. J., Saaban, S., and Clements, G. R. (2015) Melanistic leopards reveal their spots: Infrared camera traps provide a population density estimate of leopards in Malaysia, *J Wildl Manage 79*(5), 846–853. *http://doi.org/10.1002/jwmg.901*
21. Bodnar, J.-L, Riquet, D., and Houel, N. (2016) Stimulated infrared thermography applied to differentiate scar tissue from peri-scar tissue: A preliminary study, *J Med Eng Technol 40*(6), 307–314. *http://doi.org/10.1080/03091902.2016.1193239*
22. Riquet, D., Houel, N., and Bodnar, J.-L. (2019) Effect of osteopathic treatment on a scar assessed by thermal infrared camera, pilot study, *Complement Ther Med 45*, 130–135. *http://doi.org/10.1016/j.ctim.2019.06.005*
23. Barbieri, M. M., McLellan, W. A., Wells, R. S., Blum, J. E., Hofmann, S., Gannon, J., and Pabst, D. A. (2010) Using infrared thermography to assess seasonal trends in dorsal fin surface temperatures of free-swimming bottlenose dolphins (*Tursiops truncatus*) in Sarasota Bay, Florida, *Mar Mamm Sci 26*(1), 53–66. *http://doi.org/10.1111/j.1748-7692.2009.00319.x*
24. Feyer, L. J., Stewart, M., Yeung, J., Soulier, C., Whitehead, H. (2021) Origin and persistence of markings in a long-term photo-identification dataset reveal the threat of entanglement for endangered northern bottlenose whales (*Hyperoodon ampullatus*), Front. *Mar. Sci. 8. http://doi.org/10.3389/fmars.2021.620804*
25. Hicks, B. D., St. Aubin, D. J., Geraci, J. R., and Brown, W. R. (1985) Epidermal growth in the bottlenose dolphin, *Tursiops truncates, J Invest Dermatol 85*(1), 60–63. *http://doi.org/10.1111/1523-1747.ep12275348*
26. Mariani, M., Miragliuolo, A., Mussi, B., Russo G. F., Ardizzone, G., and Pace, D. S. (2016) Analysis of the natural markings of Risso's dolphins (*Grampus griseus*) in the central Mediterranean Sea, *J Mammalogy 97*(6), 1512–1524. *http://doi.org/10.1093/jmammal/gyw109*.

ABOUT STUDENT AUTHOR

Brianna Hurst graduated in May 2021 from Texas A&M University-Corpus Christi with a Bachelor's in Biology. Brianna completed the research presented as part of her National Science Foundation McNair Scholarship.

PRESS SUMMARY

A case study was conducted on the wound healing of wild common bottlenose dolphins. Two genetically and geographically distinct populations of dolphins reside in South Texas; one population occurs in the only hypersaline lagoon in the USA, while the other occurs in a hyposaline environment, providing a unique opportunity to explore how scars heal under varying natural salinities over six years. Non-invasive photography techniques were used to identify individual dolphins, and novel techniques were implemented to monitor changes in scarring, which can be widely applied to other taxa. All scars diminished among dolphins residing in the hypersaline lagoon while healing was varied in the hyposaline environment, potentially suggesting that elevated salinity augments wound healing. Scars do not appear to be stable over long durations, which has important implications for their prevalent use in photo-identification research on dolphins.

Validation of Accelerometer-Based Estimations of Energy Expenditure During High-Intensity Interval Training

Nicholas Remillard, Marisa Mulvey, Gregory Petrucci Jr, &John R Sirard**

University of Massachusetts Amherst, 30 Eastman Lane, Amherst MA 01003 and 240 Thatcher Road, Amherst, MA 01003

https://doi.org/10.33697/ajur.2022.057

Students: nremillard@umass.edu, mmulvey@ufl.edu, gpetrucci@umass.edu*
Mentor: jsirard@kin.umass.edu

ABSTRACT
Accelerometers are used to assess free-living physical activity (PA) and energy expenditure (EE). Energy expenditure estimation algorithms have been calibrated using steady-state exercise. However, most free-living PA is not steady-state. **Objective:** The purpose of this study was to discern the differences between criterion-measured and accelerometer-estimated EE (kCals) during a non-steady-state High-Intensity Interval Training (HIIT) session. **Methods:** Recreationally active adults (N=29, 18-30 years) completed one of two HIIT protocols. Each participant wore ActiGraph GT3X+ accelerometers on the right hip and non-dominant wrist while EE was measured using portable indirect calorimetry. Data analysis was conducted using custom R scripts and bias [95% CIs] to determine significant differences between indirect calorimetry and EE estimates using previously developed algorithms. **Results:** All accelerometer algorithms underestimated EE during recovery intervals (range; -4.31 to -6.55 kCals) and overestimated EE during work intervals (0.57 to 5.70 kcals). Over the whole HIIT session, only the Hildebrand wrist method was not significantly different from the criterion measured EE. **Conclusion:** Current ActiGraph EE estimations based on steady-state activities underestimate EE during recovery periods of treadmill HIIT sessions. Future studies should investigate accelerometer signals immediately after high-intensity bouts to more accurately predict EE of the subsequent recovery period.

KEYWORDS
ActiGraph; Accelerometer; HIIT; Indirect calorimetry; EPOC; Energy expenditure; Non-steady state; Calories

INTRODUCTION

Accelerometers have been used for over two decades to estimate energy expenditure (EE) and, from these estimates, categorize physical activity (PA) intensity levels, as defined by the US PA Guidelines.[1,2] Accelerometers have become a standard epidemiological tool to objectively measure physical activity and relate minutes spent in sedentary time or moderate-to-vigorous physical activity with other health behaviors and outcomes.[3–5] However, the inability of existing algorithms to estimate EE during non-steady-state activities is a known limitation.

By calibrating accelerometer EE estimation algorithms only on steady-state aerobic exercise results in a relatively narrow representation of how people exercise and perform most physical activities. Currently, no accelerometer-estimated EE algorithm considers the lag in aerobic metabolism at the beginning of a bout of exercise (oxygen deficit) or the elevated metabolism that occurs after an exercise bout (excess post-exercise oxygen consumption; EPOC). From their inception, laboratory-based accelerometer calibration studies have consistently removed the first and last minute of an exercise bout in order to only model EE from the steady-state part of the activity. Therefore, accelerometers consistently underestimate overall EE outside of structured steady-state exercise bouts, supported by one study that identified elevations in EE for 14 hours following a vigorous bout of exercise, accounting for an additional 190+71.4 kCals occurring after the exercise bout.[6-9] This accelerometer algorithm limitation is especially concerning since interval training (repeated short-duration high-intensity intervals separated by low-intensity intervals) and other forms of non-steady-state exercise have gained popularity among healthy and clinical populations.[10]

High-intensity interval training (HIIT) is broadly defined as brief (6s-4min), high intensity (85-250% VO_2 max or 90-100% HR_{max}) exercise bouts separated by similar or longer (10s-5min) recovery bouts of lower intensity (ranging from passive recovery to active recovery between 20-40% VO_2 max).[10,11] A variety of HIIT protocols have become widely accepted as an alternative form of exercise to continuous steady-state aerobic exercise, providing similar benefits, including reduced cardiometabolic disease risk factors.[10,12–16] For this initial research study, a structured HIIT session fitting the above definition of a HIIT session and including an exercise modality consistent with previous accelerometer calibration studies was used as the experimental paradigm to assess the error of accelerometer-based EE estimates during intermittent activity. Focusing this research on time periods of expected error, like EPOC, will lead to evidence that may allow for improved estimation of EE using wearable devices. Therefore, the

purpose of this proof-of-concept study was to describe the discrepancies in EE estimated from hip- and wrist-worn accelerometers during two different HIIT protocols compared with indirect calorimetry (criterion measure of EE). We hypothesized that 1) during the work intervals, hip accelerometer estimates of EE would be similar to indirect calorimetry while wrist estimates of EE would overestimate EE, 2) during recovery intervals, all accelerometer estimates would underestimate EE, resulting in 3) underestimations of total EE for all accelerometer methods over the whole HIIT session.

METHODS AND PROCEDURES

Research Design

All participants completed a preliminary and a HIIT session at least 24 hours apart and within two weeks of one another. The preliminary session was used to identify each participant's treadmill speed corresponding to 95% of their age-predicted maximal heart rate, which was used during the HIIT session for the work intervals. Two different HIIT protocols consistent with previous HIIT definitions, representing different work-to-recovery ratios (1:2 and 1:1), were conducted in independent samples. [10,11] The participants performing the first protocol completed the study prior to the larger sample of participants performing the second protocol. Protocol 1 was originally designed as a pilot study and is included in this manuscript with protocol 2 to emphasize the consistency in results. Protocol 2 improved upon protocol 1 by including an even gender distribution in a larger sample, and the different work-to-recovery ratios were included to observe potential differences in results among two common HIIT paradigms.

Participants

All participants were recruited on the University of Massachusetts Amherst campus via posted flyers, email outreach, and word of mouth. Inclusion criteria for both protocols (Protocol 1; N=9, 8 M, Protocol 2; N=20, 10 M) were 18-30 years, with a normal Body Mass Index (BMI; 18.0-24.9 $kg \bullet m^{-2}$) and physically active as defined by the Godin-Shephard Leisure-time Exercise Questionnaire, scoring 24 points or above in moderate or strenuous exercise and reported performing strenuous exercise at least once per week. [17] No participant possessed previous health conditions that would preclude their ability to participate in vigorous activity (assessed using the Physical Activity Readiness-Questionnaire [PAR-Q]).[18] In addition to the PAR-Q, participants also completed an informed consent form before the preliminary session. All study procedures were approved by the University's Institutional Review Board.

Indirect Calorimetry

The Oxycon Mobile (CareFusion Solutions, LLC, San Diego, CA) indirect calorimetry system provided the criterion measure of EE. The Oxycon Mobile is a portable gas-exchange analyzer, worn like a backpack, which includes a face mask covering the nose and mouth, sampling tubes attached to a gas analyzer, and a telemetry unit. Data from the telemetry unit was sent to a PC and processed in JLAB (CareFusion, Germany 234 Gmbh) software. The Oxycon gas analyzer was calibrated within a 3% difference with a known gas mixture of 15.98% O_2 and 3.90% CO_2, and volume calibration was completed through JLAB. Breath-by-breath O_2 and CO_2 data were collected and averaged every 5 seconds in units of mL/min.

Heart Rate

Heart rate (HR) was measured during the preliminary session using a Polar monitor (Polar Electro Oy, Kempele, Finland) strapped to the participant's chest. The research staff recorded HR values per the study protocol outlined below.

Accelerometers

Two ActiGraph GT3X+ accelerometers (ActiGraph Corp, Pensacola, FL), one on the right hip and the other on the non-dominant wrist, were used in both protocols. The ActiGraph was chosen because it is the most common accelerometer in United States' epidemiological studies measuring physical activity.[5] These locations were chosen because these are the most common wear locations for wearable accelerometer devices, and the accelerometer algorithms chosen for this study were calibrated using the right hip and non-dominant wrist locations. The accelerometers measured accelerations along three axes at a sampling rate of 80 Hz, and data were then collapsed to 1-second epochs. ActiLife 6 software was used to initialize and download devices.

Preliminary session

The goal of each preliminary session was to determine the treadmill velocity at which 95% of the maximal heart rate (HR_{max}) would be achieved, representing a vigorous intensity that fits the work interval criteria of HIIT exercise.[10] The preliminary session began with a 5-minute warm-up walking period at 4.8 km/hr. Then, participants were instructed to run at 8.9, 9.7, and 10.5 km/hr for two minutes each. Three HR data points were collected at each of the three velocities (at 40 seconds, 80 seconds, and 120 seconds), and the average of the three values was used for further calculations. After the final running bout, participants were instructed to engage in a cool-down period for 5-minutes at 4.8 km/hr. A linear fit of HR over treadmill speed was used to estimate the speed at which the participant would attain 95% of their age-predicted HR_{max} (HR_{max}=220-age).[19,20]

HIIT session

Participants were required to fast for 4 hours prior to the HIIT session to ensure that the EE predictions were attributed to physical activity energy expenditure (PAEE) rather than diet-induced thermogenesis. The HIIT session began with a 5-minute warm-up at 4.8 km/hr, followed by the HIIT intervals when participants alternated between five work intervals and five recovery intervals. Participants ran at the calculated velocity from the preliminary session during work intervals and walked at 4.8 km/hr during the recovery intervals. Protocol 1 (N=9) consisted of 45-second work intervals and 90-second recovery intervals (1:2 work-to-recovery ratio), totaling 11 minutes and 15 seconds of interval training. Protocol 2 (N=20) consisted of 1-minute work intervals and 1-minute recovery intervals (1:1 work-to-recovery ratio), totaling 10 minutes of interval training. All interval sessions were followed by a 5-minute walking cool-down at 4.8 km/hr (see Figure 1).

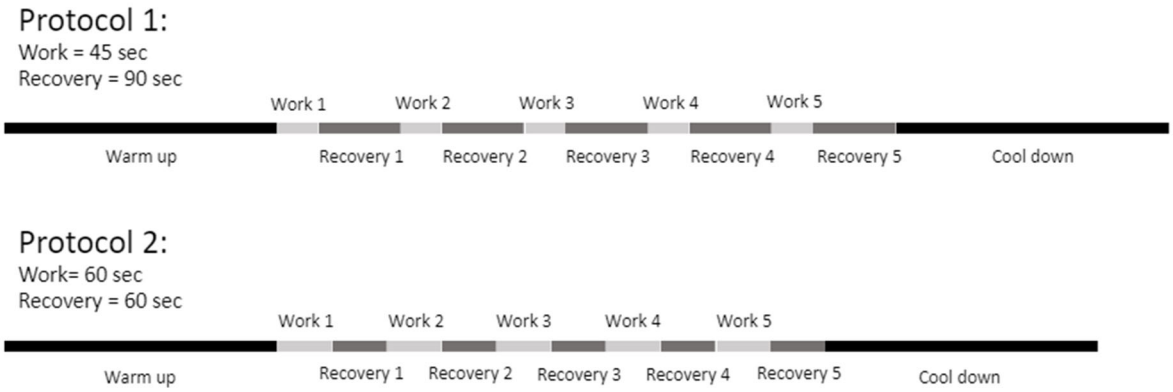

Figure 1. Sequence of events for Protocol 1 (1:2) and Protocol 2 (1:1)

Data Processing

The Oxycon Mobile collected breath-by-breath data during the entire exercise session, including warm-up and cool-down, and was reported in 5-second epochs, which represented the rate of oxygen consumption, in mL/min, for each 5-second epoch. Only data between the start of the first work interval to the end of the last rest interval was extracted for analysis. The average of twelve data points (epochs) provided the average oxygen consumption per minute. Minute-by-minute oxygen consumption data was converted to EE, in kCals/minute, using *the Weir Equation:* [21]

$$EE\ (kCals/minute) = [3.94*(VO_2\ in\ L/min)]+[1.11*(VCO_2\ in\ L/min)]$$

Four common accelerometer-based EE prediction algorithms were compared with our criterion measure, each using different accelerometer processing or location. To match the 5-second metabolic data, ActiGraph data (counts) were summed for each 5-second epoch, synchronous with the Oxycon Mobile data. The ActiGraph counts per 5-second epoch were then summed to create counts per minute data by summing twelve consecutive 5-second epochs. Vertical count data from the hip-worn ActiGraph were converted to relative units of energy expenditure using the *Freedson Equation*, where BW (body weight) is measured in kilograms (kg):[1]

$$EE\ (kCals/minute) = [(0.00094)(counts/min)]+[(0.1346)(BW)]-(7.37418)$$

The ActiGraph hip VM (vector magnitude; incorporating all three axes) count data were converted with the *Sasaki Equation*, producing EE predictions expressed in METs per minute:[22]

$$EE\ (METs/minute) = (0.000863*VM)+0.668876$$

METs per minute were then converted into kCals per minute using the following equation, where BW is measured in kg (https://sites.google.com/site/compendiumofphysicalactivities/help/unit-conversions):

$$EE\ (kCals/minute) = (METs*3.5*BW)/200$$

In addition to equations using count data, raw acceleration data from the hip and wrist were translated to Euclidian Norm Minus One (ENMO) units (R-code used to calculate ENMO can be found in Hildebrand et al., 2014) and then to VO_2 using the Hildebrand hip and wrist equations.[23] Both equations produce VO_2 ($mLO_2/kg/min$) using the ENMO data (mg = ENMO*1000):

$$\text{Hip: } VO_2\ (mLO_2/kg/min) = 0.0554*(mg)+6.67$$
$$\text{Wrist: } VO_2\ (mLO_2/kg/min) = 0.0320*(mg)+7.28$$

Resulting VO_2 from the Hildebrand equations was converted to kCals per minute using the Weir equation, including only VO_2:

$$kCals/minute = 5*(VO_2 \text{ in L } O_2/min)*BW$$

Data Analysis

Software-specific output files from the Oxycon Mobile and ActiLife were converted to CSV files, and custom R scripts were used for all data processing and analyses. No data from the warm-up or cool-down periods are included in the analyses. Analyses were performed separately for each protocol since they were not designed to be iso-caloric. ActiGraph-estimated EE has been plotted along with the measured EE calculated from the oxygen consumption data to visualize EE patterns during the HIIT sessions. Descriptive analyses indicated that the data approximated a normal distribution for all statistical tests.

To assess the criterion validity of accelerometer-based EE estimates during the HIIT protocols, the difference (bias) between ActiGraph-estimated EE and indirect calorimetry was calculated. Separate bias estimates were calculated for the differences in EE across the whole HIIT session, just the work intervals and just the recovery intervals. Mean bias and 95% bias intervals that did not span zero defined significant differences between ActiGraph-estimated and indirect calorimetry measured EE. Bias values above zero indicate an ActiGraph overestimation, and bias values below zero indicate an Actigraph underestimation.

RESULTS

Based on the participant inclusion criteria, the samples for both protocols were similar in mean age and range (18 to 30 years for both samples) with normal BMI values and considered regularly active. Protocol 1 consisted of mostly males, while Protocol 2 had an even split between male and female participants (Table 1). All analyses in this paper were conducted, including both male and female participants together. There were observed absolute differences between the sexes, but the sex-specific bias estimates were similar to the full sample, so sex-separate analyses are not included here.

	Weight (kg)	Height (m)	BMI (kg/m^2)	Age (yrs)	Godin-Shepard Score (units)	Treadmill Work Speed (kmh)
Protocol 1 (N=9, 8 male)	75.5 ± 10.9	1.7 ± 0.1	24.7 ± 3.7	20.4 ± 1.7	71.7 ± 16.6	12.8 ± 1.9
Protocol 2 (N=20, 10 male)	70.0 ± 7.7	1.7 ± 0.1	24.4 ± 2.9	20.7 ± 1.9	65.5 ± 14.3	12.1 ± 2.0

Table 1. Participant Characteristics (Mean ± SD).

Figure 2 provides a visualization of the ActiGraph and oxygen consumption data during the full duration of the HIIT sessions for Protocol 1 (panels A and C) and Protocol 2 (panels B and D). The accelerometer data clearly demonstrates an instantaneous response to movement changes, while the metabolic data show a lagged increase in O_2 consumption at the beginning of each work interval and a delay in the decline in O_2 consumption during the recovery intervals (demonstrating the effects of EPOC).

Figure 3 provides mean kCals, by method, for each work and rest interval for both protocols. Error bars are not presented to ease the readability of the figure. Supplemental Table 1 (Table S1) contains means and standard deviations for each work and recovery bout for both protocols. Consistent with the unprocessed data in Figure 1, EE measured with indirect calorimetry is greater during the recovery intervals due to EPOC compared with EE values during the work intervals. The difference in work-to-recovery ratios between protocols (protocol 1, 1:2; protocol 2, 1:1) explains the significantly higher EE values during Protocol 1 recovery intervals as compared to Protocol 2 recovery intervals ($p < 0.001$; two-sample heteroscedastic T-test to compare criterion measured EE between protocols).

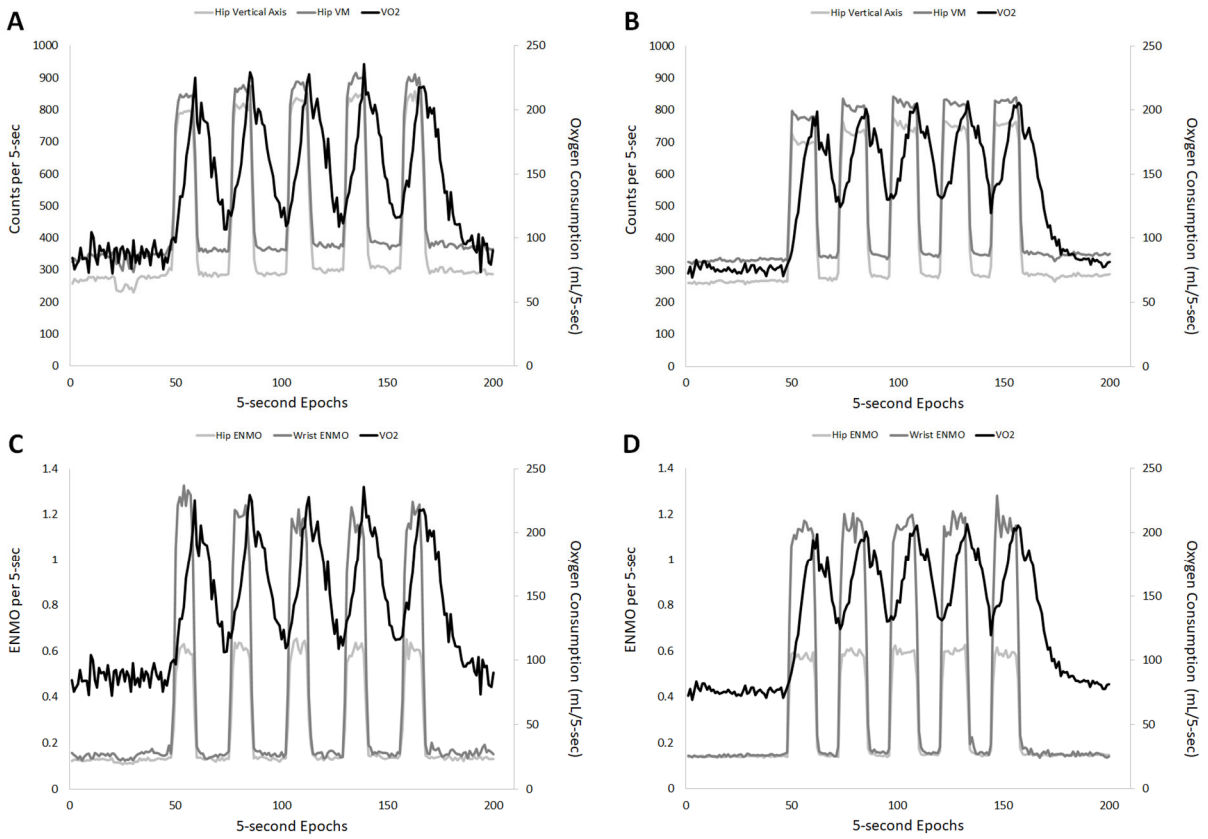

Figure 2. Mean accelerometer counts/5-sec interval for the hip vertical axis and hip VM (primary axis), as well as the rate of oxygen consumption (secondary axis; mL O_2/5-sec), are shown in Panel A (protocol 1) and Panel B (protocol 2). Hip and wrist ENMO data per 5-sec interval (primary axis), as well as the rate of oxygen consumption (secondary axis; mL O_2/5-sec), are shown in Panel C (protocol 1) and Panel D (protocol 2).

Total EE (kCals; mean (SD)) measured by the criterion measure for the entire HIIT session (calculated from the beginning of Work 1 through the end of Recovery 5) for Protocol 1 and Protocol 2 were 107.8 (19.5) kCals and 98.9 (24.7) kCals, respectively. Bias and 95% confidence interval estimates for each method, for the whole HIIT session (total), and separated into work and recovery intervals are presented in Table 2. Graphical representations of bias for each method can be found in Supplemental Figures S1-S4.

The Freedson algorithm significantly overestimated work EE for Protocol 1 (bias in kCals, 1.69), but not Protocol 2 (0.57); underestimated recovery EE for both protocols (-4.66 and –4.41); and therefore, underestimated total EE for both protocols (-14.82 and –19.25). For both protocols, the Sasaki and Hildebrand hip algorithms both significantly overestimated work EE (range, 1.30 to 4.00) and underestimated recovery EE (range, -4.31 to –5.63). The Sasaki algorithm underestimated total EE for both protocols (-11.77 and –15.08), while the underestimation of total EE using the Hildebrand hip algorithm was significant for protocol 1 (-8.15) but not for protocol 2 (-1.83). The Hildebrand wrist algorithm produced the greatest work EE overestimations (5.00 and 5.70) and the greatest recovery EE underestimations (-6.55 and -5.14). The Hildebrand wrist under- and overestimations canceled each other out such that there was no significant difference in total EE for either protocol (-7.76 and 2.79) compared with indirect calorimetry.

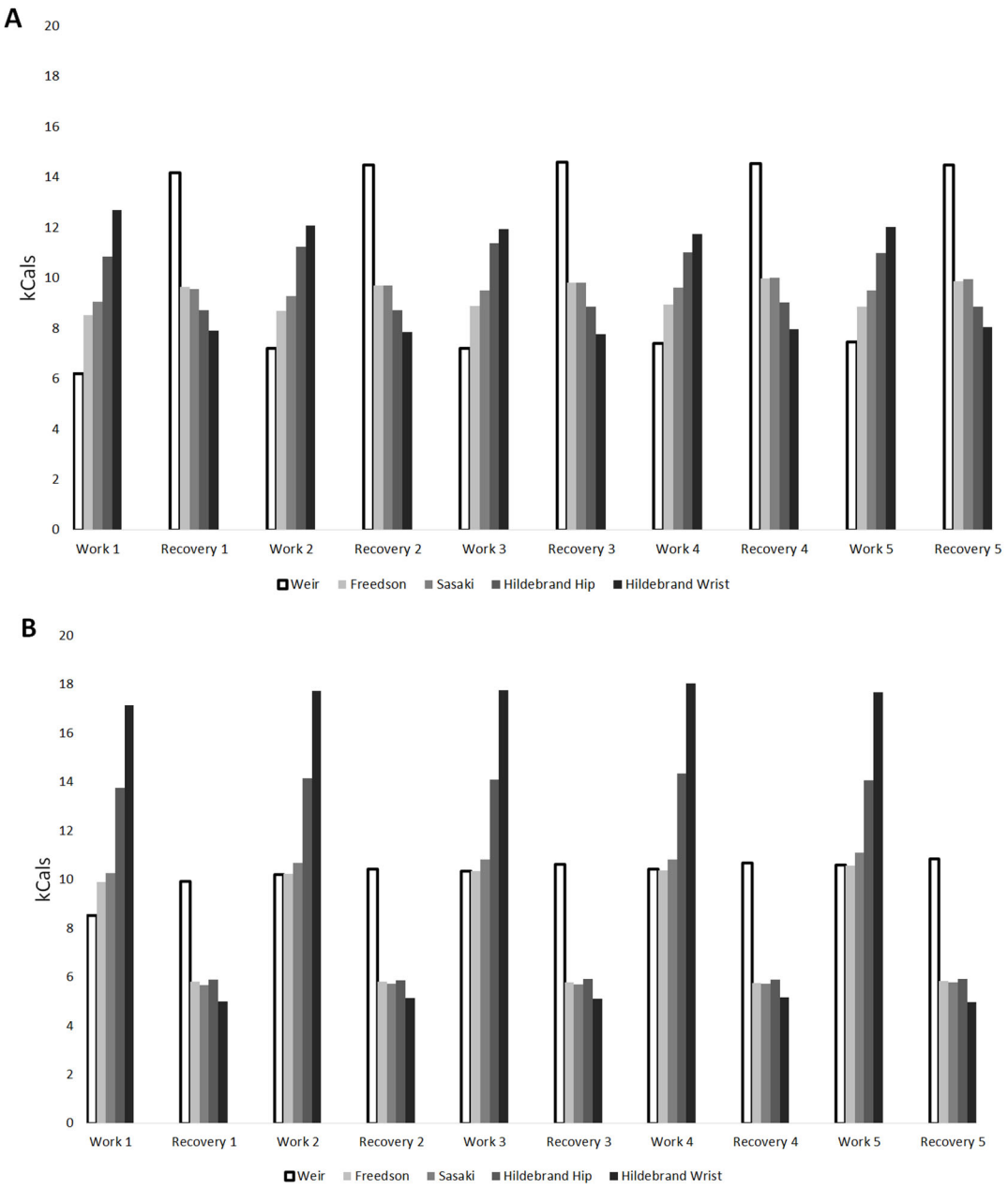

Figure 3. Energy expenditure (EE) in kCals/interval calculated from oxygen consumption data (criterion using the Weir equation) and the accelerometer prediction equations, Freedson Hip, Sasaki Hip, Hildebrand Hip, and Hildebrand Wrist for protocol 1 (panel A) and protocol 2 (panel B).

DISCUSSION

The purpose of this study was to characterize the discrepancies between accelerometer-estimated EE and indirect calorimetry during two HIIT protocols. Overall, most ActiGraph EE equations overestimated EE during work intervals and underestimated it during recovery intervals. Considering the total EE over the whole protocols, the Freedson equation underestimated EE for both protocols, the Hildebrand wrist equation was not biased for either protocol, and the Sasaki and Hildebrand hip equations underestimated for one protocol and were not biased for the other. These results have implications for the research community and for individuals wearing commercial-grade accelerometer devices.

To our knowledge, no other study has compared indirect calorimetry with accelerometer-estimated EE during the separate work and recovery intervals of intermittent exercise. However, the current findings are supported by previous free-living accelerometer validation studies that have tested existing algorithms to estimate EE using indirect calorimetry.[24–26] These previous studies have found that, for lifestyle activities like racquetball, basketball, and tennis, which involve intermittent movement, the Freedson

prediction equation underestimated kCals as compared with indirect calorimetry. Underestimation during these studies ranged from –1.0 kCals/min to –5.5 kCals/min. In contrast, the validation studies considering steady-state ambulatory activities found less bias (between -0.8 and 1.8 kCals/min) using the Freedson equation, suggesting that existing energy expenditure estimation equations may be fairly accurate during steady-state treadmill activities.[24,26] Despite differences in protocols across studies, the underestimation of EE found during these intermittent leisure-time sports activities and ADLs support our findings from the current HIIT protocols and further indicates the need to develop more specific EE algorithms targeting intermittent activities. Because these previous studies only assessed the simulated free-living activity sessions as a whole, it remains unclear what during the session was driving the underestimation of EE during these studies.[24–26] The current study is novel in using the HIIT paradigm as a substitute for intermittent lifestyle activities and breaking up the activity period into work and recovery intervals to determine if undetected elevated EE during recovery intervals is responsible for accelerometer EE biases.

Kcals/min	Method	Protocol 1 Bias [95% C.I.]	Protocol 2 Bias [95% C.I.]
Total	Freedson	-1.32 [-2.41, -0.23] *	-1.92 [-2.83, -1.02] *
	Sasaki	-1.05 [-2.36, 0.26]	-1.51 [-2.44, -0.58] *
	Hildebrand Hip	-0.72 [-1.42, -0.02] *	-0.18 [-0.88, 0.51]
	Hildebrand Wrist	-0.69 [-1.64, 0.26]	0.28 [-0.64, 1.20]
Work	Freedson	2.26 [0.42, 4.1] *	0.57 [-0.49, 1.63]
	Sasaki	3.07 [0.61, 5.53] *	1.30 [0.24, 2.36] *
	Hildebrand Hip	5.33 [3.91, 6.75] *	3.98 [3.30, 4.66] *
	Hildebrand Wrist	6.67 [4.53, 8.81] *	5.70 [3.53, 7.87] *
Recovery	Freedson	-3.10 [-3.91, -2.29] *	-4.41 [-5.24, -3.58] *
	Sasaki	-3.10 [-3.98, -2.22] *	-4.31 [-5.23, -3.39] *
	Hildebrand Hip	-3.75 [-4.48, -3.02] *	-4.34 [-5.22, -3.46] *
	Hildebrand Wrist	-4.37 [-5.15, -3.59] *	-5.14 [-5.96, -4.32] *
Kcals/interval	**Method**	**Protocol 1 Bias [95% C.I.]**	**Protocol 2 Bias [95% C.I.]**
Total	Freedson	-14.82 [-27.1, -2.54] *	-19.25 [-28.27, -10.23] *
	Sasaki	-11.77 [-26.55, 3.01]	-15.08 [-24.4, -5.76] *
	Hildebrand Hip	-8.15 [-15.98, -0.32] *	-1.83 [-8.8, 5.14]
	Hildebrand Wrist	-7.76 [-18.45, 2.93]	2.79 [-6.43, 12.01]
Work	Freedson	1.69 [0.32, 3.06] *	0.57 [-0.49, 1.63]
	Sasaki	2.30 [0.45, 4.15] *	1.30 [0.24, 2.36] *
	Hildebrand Hip	4.00 [2.94, 5.06] *	3.98 [3.30, 4.66] *
	Hildebrand Wrist	5.00 [3.40, 6.60] *	5.70 [3.53, 7.87] *
Recovery	Freedson	-4.66 [-5.88, -3.44] *	-4.41 [-5.24, -3.58] *
	Sasaki	-4.65 [-5.97, -3.33] *	-4.31 [-5.23, -3.39] *
	Hildebrand Hip	-5.63 [-6.72, -4.54] *	-4.34 [-5.22, -3.46] *
	Hildebrand Wrist	-6.55 [-7.72, -5.38] *	-5.14 [-5.96, -4.32] *

Table 2. kCal bias (ActiGraph EE estimate – criterion) by interval and method; *significantly different from zero ($p<0.05$).

In the current study, the underestimation of EE during recovery intervals was primarily responsible for the overall EE underestimation of the HIIT session for most methods. These findings may also apply to consumer wearables, which often produce EE underestimations (mean: -3%; median: -11%) when compared to indirect calorimetry.[6,7,27] The greatest underestimations produced by consumer wearables are reported during the highest intensity intermittent activities (e.g., basketball, tennis), suggesting that if worn for long periods at a time, highly active wearers would experience greater levels of EE underestimation than sedentary or low active wearers. If the results of the current study were extrapolated, a 60-minute interval-like activity of equivalent intensity could be underestimated by as much as 88 kCals (using the Freedson equation) and does not consider the slow phase of EPOC. Our results are directly applicable to the Freedson, Sasaki, and Hildebrand algorithms used with the ActiGraph but may apply to other research- and consumer-grade devices and algorithms.

This study had several strengths. Two separate protocols were completed in independent samples with similar results obtained from both. This suggests that regardless of the work-to-recovery ratio, accelerometer-based EE estimates from other HIIT protocols would reflect similar results to those in the current study. Additionally, the synchronization of the accelerometer and oxygen consumption data ensures that the current results are not due to discrepancies in data collection timing. Also, the wear locations make these results applicable to larger-scale epidemiology studies and to surveillance efforts using the ActiGraph.

One limitation of this study is that there was no long-term follow-up after the cessation of exercise to observe the slow component of EPOC on overall EE. Future studies could include a prolonged follow-up after interval training or other exercise or sports events. Also, both protocols had relatively small sample sizes (N=9 and N=20, respectively), which runs the risk that these results may not be replicated if the protocols were repeated with larger samples. Protocol 2 had an equal distribution of males and females, although protocol 1 only had one female participant, which could be considered a limitation. However, both protocols yielded similar results. The sample for both protocols included only healthy, young adults; therefore, it is possible that these results might not be applicable to other populations, such as sedentary adults, older adults, and children. Concerning the treadmill, safety was a priority, and so the protocols described in this study were limited to participant speeds at 95% of their HR max, which often translated to a fast jog or slow run for our participants. These results cannot be generalized to all types of HIIT training, such as body weight-centered circuit training or sprint interval training (defined as maximum all-out effort bouts).

CONCLUSIONS

In conclusion, this study affirms that estimations of EE converted from ActiGraph accelerometer data are underestimated during high-intensity interval training and identifies a specific source of error in the post-exercise time period that can be targeted in the future device calibration efforts. This error could be substantial for highly active individuals who perform interval-like exercise or sports, leading to discrepancies that could have meaningful over-or under-estimations of people's free-living behavior in many research studies that use the ActiGraph, and potentially other research- and consumer-grade activity trackers. Future research should 1) modify the intensity and duration of work and rest intervals to study the effects on EE estimates and 2) incorporate a longer post-exercise recovery period to more precisely estimate the contribution of the EPOC slow component to daily EE estimates. Continuing this line of research would further improve algorithms used to estimate EE from accelerometer data and could potentially be used to inform improvements to EE estimates of consumer activity tracking devices.

ACKNOWLEDGEMENTS

This research was funded by two University of Massachusetts Amherst Commonwealth Honors College Research Grants.

DECLARATION OF INTEREST

The authors declare that they have no known competing financial interests or personal relationships that could have appeared to influence the work reported in this paper.

REFERENCES

1. Freedson PS, Melanson E, Sirard J. (1998) Calibration of the Computer Science and Applications, Inc. accelerometer. *Med Sci Sports Exerc.* 30(5):777-781. *doi:10.1097/00005768-199805000-00021*
2. Piercy KL, Troiano RP, Ballard RM, et al. (2018) The physical activity guidelines for Americans. *Jama.* 320(19):2020-2028.
3. Garriguet D, Tremblay S, Colley RC. (2015) Comparison of Physical Activity Adult Questionnaire results with accelerometer data. *Heal reports.* 26(7):11.
4. Lee IM, Shiroma EJ. (2014) Using accelerometers to measure physical activity in large-scale epidemiological studies: Issues and challenges. *Br J Sports Med.* 48(3):197-201. *doi:10.1136/bjsports-2013-093154*
5. Troiano RP, Berrigan D, Dodd KW, et al. (2008) Physical activity in the United States measured by accelerometer. *Med Sci Sports Exerc.* 40(1):181.
6. Adam Noah J, Spierer DK, Gu J, Bronner S. (2013) Comparison of steps and energy expenditure assessment in adults of Fitbit Tracker and Ultra to the Actical and indirect calorimetry. *J Med Eng & Technol.* 37(7):456-462.
7. Fuller D, Colwell E, Low J, et al. (2020) Reliability and validity of commercially available wearable devices for measuring steps, energy expenditure, and heart rate: systematic review. *JMIR mHealth uHealth.* 8(9):e18694.
8. Panissa VLG, Fukuda DH, Caldeira RS, et al. (2018) Is oxygen uptake measurement enough to estimate energy expenditure during high-intensity intermittent exercise? Quantification of anaerobic contribution by different methods. *Front Physiol.* 9:868.
9. Knab AM, Shanely RA, Corbin KD, Jin F, Sha W, Nieman DC. (2011) A 45-minute vigorous exercise bout increases metabolic rate for 14 hours. *Med Sci Sport Exerc.* 43(9):1643-1648.
10. Batacan RB, Duncan MJ, Dalbo VJ, Tucker PS, Fenning AS. (2017) Effects of high-intensity interval training on cardiometabolic health: a systematic review and meta-analysis of intervention studies. *Br J Sports Med.* 51(6):494-503.
11. Norton K, Norton L, Sadgrove D. (2010) Position statement on physical activity and exercise intensity terminology. *J Sci Med Sport.* 13(5):496-502.
12. Buchheit M, Laursen PB. (2013) High-intensity interval training, solutions to the programming puzzle. *Sport Med.* 43(5):313-338.
13. Sawyer BJ, Tucker WJ, Bhammar DM, Ryder JR, Sweazea KL, Gaesser GA. (2016) Effects of high-intensity interval

training and moderate-intensity continuous training on endothelial function and cardiometabolic risk markers in obese adults. *J Appl Physiol.* 121(1):279-288.
14. Wewege M, Van Den Berg R, Ward RE, Keech A. (2017) The effects of high-intensity interval training vs. moderate-intensity continuous training on body composition in overweight and obese adults: a systematic review and meta-analysis. *Obes Rev.* 18(6):635-646.
15. Zhang H, Tong TK, Qiu W, et al. (2017) Comparable effects of high-intensity interval training and prolonged continuous exercise training on abdominal visceral fat reduction in obese young women. *J Diabetes Res.* 2017.
16. Keating SE, Johnson NA, Mielke GI, Coombes JS. (2017) A systematic review and meta-analysis of interval training versus moderate-intensity continuous training on body adiposity. *Obes Rev.* 18(8):943-964.
17. Godin G. (2011) The Godin-Shephard leisure-time physical activity questionnaire. *Heal & Fit J Canada.* 4(1):18-22.
18. Warburton DER, Gledhill N, Jamnik VK, et al. (2011) Evidence-based risk assessment and recommendations for physical activity clearance: Consensus Document 2011. *Appl Physiol Nutr Metab.* 36(S1):S266--S298.
19. Åstrand P-O, Åstrand I. (1958) Heart rate during muscular work in man exposed to prolonged hypoxia. *J Appl Physiol.* 13(1):75-80.
20. Powers SK, Howley ET, Quindry J. (2007) *Exercise Physiology: Theory and Application to Fitness and Performance*. McGraw-Hill New York, NY.
21. Weir JB de V. (1949) New methods for calculating metabolic rate with special reference to protein metabolism. *J Physiol.* 109(1-2):1-9.
22. Sasaki JE, John D, Freedson PS. (2011) Validation and comparison of ActiGraph activity monitors. *J Sci Med Sport.* 14(5):411-416. *doi:10.1016/j.jsams.2011.04.003*
23. Hildebrand M, Van Hees VT, Hansen BH, Ekelund U. (2014) Age group comparability of raw accelerometer output from wrist-and hip-worn monitors. *Med Sci Sports Exerc.* 46(9):1816-1824. *doi:10.1249/MSS.0000000000000289*
24. Crouter SE, Churilla JR, Bassett DR. (2006) Estimating energy expenditure using accelerometers. *Eur J Appl Physiol.* 98(6):601-612. *doi:10.1007/s00421-006-0307-5*
25. Imboden MT, Nelson MB, Kaminsky LA, Montoye AH. (2018) Comparison of four Fitbit and Jawbone activity monitors with a research-grade ActiGraph accelerometer for estimating physical activity and energy expenditure. *Br J Sports Med.* 52(13):844-850. *doi:10.1136/bjsports-2016-096990*
26. Lyden K, Kozey SL, Staudenmeyer JW, Freedson PS. (2011) A comprehensive evaluation of commonly used accelerometer energy expenditure and MET prediction equations. *Eur J Appl Physiol.* 111(2):187-201.
27. Sasaki JE, Hickey A, Mavilia M, et al. (2015) Validation of the Fitbit wireless activity tracker for prediction of energy expenditure. *J Phys Act Heal.* 12(2):149-154.

ABOUT THE STUDENT AUTHORS

This data was collected, and the majority of the manuscript was written by Nicholas Remillard and Marisa Mulvey during their senior years of their undergraduate studies. As his undergraduate honors thesis, Nicholas Remillard developed the research question and study protocols under the guidance of his mentor John Sirard and master's student Greg Petrucci. Marissa Mulvey continued data collection and improved upon the original study protocol for her undergraduate honors thesis, and both Nicholas Remillard and Marissa Mulvey collaborated on data analyses and the writing of the manuscript.

PRESS SUMMARY

Measuring energy expenditure is critical in understanding physical activity's relationship with health and disease. Currently, there is no way to directly measure energy expenditure outside of laboratory settings. Existing energy expenditure prediction algorithms based on wearable devices inaccurately estimate energy expenditure outside of controlled laboratory conditions. The current study identified the post-exercise time period as a source of underestimation of energy expenditure from the wearable device algorithms. This underestimation could be substantial for highly active individuals who perform interval-like exercise or sports and rely on a wearable device to track their calories burned. In addition, the results of this study demonstrate current limitations that should be considered by researchers studying the metabolic effects of high-intensity exercise using wearable devices.

Print Edition ISSN 1536-4585
Online Edition ISSN 2375-8732